NONLINEAR DYNAMICS
OF THE
HEART RATE VARIBILITY SIGNAL

NONLINEAR DYNAMICS OF THE HEART RATE VARIABILITY SIGNAL

By
NESRENE SHAWKI SALEM, B.ENG

A Thesis Submitted to
the School of Graduate Studies
in Partial Fulfillment of the Requirements
for the Degree
Master of Engineering

McMaster University
©Copyright by Nesrene Shawki Salem, August 2001

Master of Engineering (2001) McMaster University

(Electrical and Computer Engineering) Hamilton, Ontario

TITLE: Nonlinear Dynamics of the Heart Rate Variability Signal

AUTHOR: Nesrene Shawki Salem, B.Eng. (The Arab Academy for Science and Technology)

SUPERVISOR: Dr. Markad V. Kamath, Ph.D., P.Eng.

NUMBER OF PAGES: xii, 97

To my parents Shawki Salem and Samia Salem,

and my sister Mayada.

Abstract

The heart rate variability (HRV) signal has been employed as a measure of sympathovagal balance in the human autonomic nervous system (ANS). It is known that aging affects the functional characteristics of the ANS. It has been suggested that complexity as measured by nonlinear dynamical indices, decays with age. We developed several algorithms and test protocols to characterize nonlinear dynamics in the HRV signal and to test the hypothesis that aging reduces the complexity within the HRV signal.

Continuous HRV signal was obtained from 93 healthy subjects (41 males and 52 females) ranging in age between 5 and 78 years under controlled laboratory conditions in supine state. Subjects were from pediatric (PED, 5-12 years, n=15, 9 male, 6 female), adolescent (ADO, 13-17 years, n=16, 6 male, 10 female), adult (ADL, 18-30 years, n=22, 12 male, 10 female), middle aged (MDA, 31-60 years, n=21, 8 male, 13 female) and elderly (ELD, 61+ years, n=19, 6 male, 13 female) age groups. The length of data was 1000 or more R-R intervals for adequate computation. Stationary Holter HRV data from these controls were also used for the present study.

Our results are as follows: There is a continuous systematic decay in the power-law scaling (β), which decreases from -1.162 ± 0.388 for the PED group to -1.95 ± 0.6 for the ELD group ($F = 6.649$, $p < 0.001$; R = 0.475, $p < 0.001$. Approximate entropy

(ApEn) decreases with age from 1.456 ± 0.093 for the PED group to 1.272 ± 0.135 for the ELD group (F = 7.82, p < 0.001; R = 0.519, p < 0.001. The detrended fluctuation analysis (DFA) of short-term data yielded an increase in short-range DFA scaling exponent α_1 from 0.774 ± 0.204 for the PED group to 1.138 ± 0.289 for the ELD group (F = 7.535, p < 0.001), and in long-range DFA scaling exponent α_2 increased from 0.667 ± 0.082 for the PED group to 0.86 ± 0.172 for the ELD group (F = 4.841, p < 0.001). The detrended fluctuation analysis (DFA) of long-term data yielded an increase in short-range DFA scaling exponent α_1 from 1.052 ± 0.218 for the PED group to 1.204 ± 0.205 for the ELD group (F = 1.922), and in long-range DFA scaling exponent α_2 increased from 0.961 ± 0.081 for the PED group to 1.076 ± 0.102 for the ELD group (F = 4.06, p < 0.01). Surrogate data analysis demonstrated that the hypothesis that the HRV signal is generated by a linear stochastic process is not always rejected.

In summary, the HRV signal lends itself to an analysis using nonlinear dynamical methods and studies in patients may yield useful clinical information in the future.

Acknowledgements

I would like to express my appreciation to all those individuals who played a role in the completion of this thesis.

I would like to thank my supervisor Dr. Markad V. Kamath for his supervision throughout the course of this work.

In addition, I would like to express my gratitude to my sister Mayada and my friends, especially Boris and William, for their encouragement, support, and constant willingness to help me during my study at McMaster University.

I enjoyed working with Windy Li, Clement Peng, Wendy Wong and Shingo Yuki, my colleagues during graduate study at McMaster University.

It is a pleasure to acknowledge the facilities and research funds generously provided by Heart and Stroke Foundation of Ontario, de Groote Foundation and Natural Sciences and Engineering Research Council (NSERC) of Canada, for conducting the research described herein.

Above all, I want to thank my parents for inspiring me, and for their unwavering support over the years. This work could not have been accomplished without their help.

Contents

Abstract **iii**

Acknowledgements **v**

1 Introduction **1**

1.1 Introduction 1

1.2 Organization of the Thesis 4

2 Introduction to Nonlinear Dynamics and Chaos **5**

2.1 Background 5

2.2 Characteristics of Signals with Deterministic Chaos 6

3 Origin of the Heart Rate Variability Signal **8**

3.1 Physiological Background 8

3.1.1 Anatomy 8

3.1.2 Regulation of the Cardiac Activity 10

3.1.3 The Electrocardiogram (ECG) 12

3.2 The Heart Rate Variability Signal 13

4 Chaos in Physiology and Effects of Aging on Heart Rate Variability Signal **15**

4.1 Introduction 15

4.2 Evidence for the Presence of Chaos in Physiological Signals 16

4.3 HRV Signal and the Effect of Age 19

4.4 Conclusion 22

5 Indices of Nonlinear Dynamics of the HRV Signal 23

5.1 Introduction 23

5.2 Power-Law Scaling 23

5.3 Approximate Entropy 27

5.4 Detrended Fluctuation Analysis (DFA) 29

5.5 Correlation Dimension and Surrogate Data 34

5.5.1 Surrogate data analysis 34

5.5.2 Correlation dimension 36

5.6 Conclusion 37

6 ECG and HRV Signal Acquisition and Processing 38

6.1 Introduction 38

6.2 Subjects – Recruitment and Screening 38

6.3 Testing Protocol 39

6.4 Acute Recordings 39

6.5 Twenty Four-Hour Recordings 41

6.6 Signal Processing and Data Analysis 42

6.6.1 Computation of power-law scaling 44

6.6.2 Computation of approximate entropy 44

6.6.3 Computation of detrended fluctuation analysis 45

6.6.4 Computation of surrogate data and correlation dimension 45

6.7 Testing of Nonlinear Dynamic Indices 46

6.7.1 The Logistic map 46

6.7.2 Signal with added noise 49

6.7.3 Testing of power-law scaling 51

6.7.4 Testing of approximate entropy 52

6.7.5 Testing of detrended fluctuation analysis (DFA) 52

6.7.6 Testing of surrogate data 53

6.8 Statistics 58

6.9 Conclusion 58

7 Effects of Aging on the Nonlinear Dynamics of the HRV Signal 59

7.1 Introduction 59

7.2 Effects of Aging on Power-Law Scaling of the HRV Signal 59

7.3 Effects of Aging on Approximate Entropy of the HRV Signal 59

7.4 Effects of Aging on Detrended Fluctuation Analysis of the HRV Signal 63

7.4.1 Short-Term DFA 63

7.4.2 Long-Term DFA 63

7.5 Correlation Dimension of the HRV Signal 68

8 Discussion 74

8.1 Introduction 74

8.2 Effect of Age on Physiological Signals Implication: Nonlinear Techniques 74

8.3 Limitations 77

8.4 Future Research 77

9 Conclusion 78

Bibliography 80

Appendices 85

A Forms 86

B Raw Data 92

List of Figures

3.1	The Heart Structure	9
3.2	Nerve supply to the heart from the autonomic nervous system	11
3.3	QRS Complex	13
4.1	Self-similarity in fractal objects	18
5.1	Heart rate dynamics and power-law scaling aspects	26
5.2	Heart rate spectral distribution for young and old subjects	26
5.3	DFA of the R-R interval	32
6.1	The R-R interval tachograms	44
6.2	The bifurcation diagram of the logistic map	47
6.3	The logistic map	48
6.4	The artificial signals used for testing	50
6.5	Testing the power-law scaling	51
6.6	Testing the DFA scaling exponent	53
6.7	Testing the surrogate data	55
7.1	Effect of age on power-law scaling	61
7.2	Effect of age on approximate entropy	62
7.3	Scatter plot of short-term DFA	66
7.4	Scatter plot of long-term DFA	67

7.5 Correlation dimension for two subjects from the pediatric group 69

7.6 Correlation dimension for two subjects from the adolescent group 70

7.7 Correlation dimension for two subjects from the adult group 71

7.8 Correlation dimension for two subjects from the middle aged group 72

7.9 Correlation dimension for two subjects from the elderly group 73

List of Tables

6.1 Testing approximate entropy 52

7.1 The values of β according to each age group 60

7.2 The values of ApEn according to each age group 60

7.3 The values of short-term scaling exponents α_1 and α_2 according to each age group 65

7.4 The values of long-term scaling exponents α_1 and α_2 according to each age group 65

Chapter 1

Introduction

1.1 Introduction

There has been much recent interest in the analysis of heart rate variability (HRV) signal in a variety of clinical settings. Several well-known techniques have been applied to analyze the HRV signal [1, 2, 3, 4]. These include the following: first, time domain measures of heart rate variability, and second, the spectral analysis that expresses the HRV signal in the frequency domain. Both time and frequency domain HRV measures have proven useful for clinical purposes. However, time and frequency domain measures of the HRV signal have limited value in uncovering more complex nonlinear systems [5,6]. It is likely that the HRV signal may contain elements of nonlinear dynamics, which may be better-understood using techniques of deterministic chaos. Therefore, a third group of techniques based on nonlinear system theory ('chaos theory and fractals') have been recently developed to quantify the complex HR dynamics and to complement the conventional measures of HR variability [4].

The discipline of nonlinear dynamics has been applied to many areas of physical and biological sciences [7]. Its application to cardiology may provide an innovative tool to aid our understanding of many physiologic phenomena that heretofore were deemed

inexplicable using conventional methodologies [1]. The theories of "chaos" and complexity have been developed to understand diverse fields including physics, experimental mathematics, evolutionary biology and social sciences. The common theme from such research is to understand how systems, that are inherently complex, undergo changes over time. Traditional linear science describes scientific laws where, if we know the initial starting condition of a system and the linear laws governing its behaviour, we can predict its state over time with a fair degree of confidence. Linear theory in general, is the basis for many controlled experiments. However, the presence of 'chaos' and complexity suggest that much of the world, and in particular physiology, is not linear and small changes can produce dramatic transformation of an entire system [2].

Physicians often describe the normal activity of the heart as "regular sinus rhythm". But it is now acknowledged that normal sinus rhythm in healthy individuals is a result of complex interactions between multiple regulatory processes that operate over different time scales. These include the sympathetic and parasympathetic nervous systems, which regulate beat-to-beat heart rate (HR) and blood pressure (BP), as well as cardiovascular volume, and body temperature [3]. Interactions between these control systems generate highly variable and complex beat-to-beat fluctuations that are consistent with deterministic chaos. We believe that, nonlinear dynamics and chaos theory provide techniques to measure the complexity of physiologic variability that enables us to study the effect of age on neurocardiac control in healthy human subjects.

The process of aging has a dramatic and profound impact on the complex dynamics of healthy physiologic function. This is evident in many physiologic systems,

but the cardiovascular system has received the most attention because of high morbidity and mortality associated with cardiovascular disease, and the current availability of continuous noninvasive hemodynamic data (e.g.: HR & BP) along with the development of sophisticated signal processing techniques.

It is now believed that, when a physiologic system ages, it becomes less complex and its information content is reduced. As a result, such a system is less able to cope with the exigencies of a constantly changing environment [18]. Thus, a compelling argument can be made to employ nonlinear dynamics/chaos theory to the heart rate signal in order to gain insights into physiological mechanisms that are affected as the human being ages.

Therefore, the purpose of this thesis is to analyze the HRV signal by means of methods derived from nonlinear dynamics, as well as to address a variety of questions:

- What does nonlinear dynamics offer the physician with regard to understanding normal physiology?
- How can nonlinear indices of HRV quantitate the effect of aging on HRV signal?
- Do nonlinear indices of HRV have short-term predictive value, in addition to time and frequency indices? To address these questions, we studied ApEn, a measure of complexity, DFA, an index that describes the presence or absence of long-term fractal correlations, correlation dimension, and surrogate data analysis.

1.2 Organization of the Thesis

We begin in chapter 2 by identifying some methodological issues of nonlinear dynamics and chaos theory. Chapter 3 describes some theoretical preliminaries, which describe basic concepts underlying the signals used herein, the ECG and the heart rate variability (HRV) signal. In chapter 4, a brief literature review on the effect of age on nonlinear complexity is presented. Nonlinear indices techniques are introduced in chapter 5. The process of the ECG signal acquisition, computation of the heart rate variability (HRV) signal and testing of the various techniques are discussed in chapter 6. The results of applying nonlinear dynamical techniques to the heart rate variability (HRV) signal are described in chapter 7. In chapter 8 we will analyze and compare the results of these techniques. Finally we will summarize the results of our work on the effects of aging on the heart rate variability (HRV) signal in Chapter 9.

Chapter 2

Introduction to Nonlinear Dynamics and Chaos

2.1 Background

The possibility of applying nonlinear methods to describe dynamical systems was initially contemplated by the French mathematician Henri Poincaré in the nineteenth century. However, the concept did not gain broad recognition amongst scientists until T. Y. Li and J. Yorke introduced the term "chaos" in 1975 in their analysis of the quadratic map [7]. Modeling of biological systems are often viewed as linear. The simplicity of linear systems is so attractive that investigators routinely attempt to "linearize" complex sets of data by various transformations. This practice, however, may misrepresent the true state of a system, and as a result, the underlying pathologic process, may be overlooked. Linear equations describe a one-to-one correspondence between input and output values of systems under study [1]. However, this is not the case with nonlinear equations, which are of two types, monotonic and folded. Monotonic equations are always decreasing or always increasing. In contrast, folded nonlinear equations change direction and therefore, a single output value can be associated with two or more input values. Such ambiguity gives rise to chaos under some conditions [1]. The search for chaotic dynamics in diverse physical and biological and medical fields, as well as the mathematical analysis of chaotic dynamics in nonlinear equations, has sparked extensive research into chaos, in recent years.

2.2 Characteristics of Signals with Deterministic Chaos

Chaos is best understood by comparing it to two other characteristics of signals – randomness and periodicity. A random waveform never repeats itself because it is inherently unpredictable and disorganized. We can predict the average behaviour of a random signal over a certain time frame but we cannot predict the behaviour of a single epoch of the signal. Similarly, we can compute and predict the mean heart rate, but we cannot predict future values of a set of R-R intervals in a distant time. Periodic behaviour, on the other hand is highly predictable because it constantly repeats itself over some finite period of time. Systems exhibiting periodic behaviour are governed by an underlying deterministic process. Chaos is distinct from periodicity and randomness, but it has some characteristics of both. Although a chaotic signal may look like a random signal, it is deterministic to some extent, like a periodic signal [1].

Chaotic signal exhibits a number of characteristics that distinguishes it from periodic and random signals. These include the following:

1. Chaos is both deterministic and aperiodic. Aperiodic patterns imply that the same state is not repeated. Deterministic behaviour suggests that there is a definite rule to describe the signal with no random terms governing the dynamics. Hence, we conclude that there is an underlying set of mathematical equations that controls the behaviour of the system. If one knows these equations and the initial conditions, one can predict its behaviour to some finite time. However, a chaotic signal never repeats itself exactly [1,7].

2. Chaotic systems exhibit sensitive dependence on initial conditions. Very small differences in initial conditions will result in large differences in its behaviour at a later point in time. This is an essential aspect of chaos. It means that we may be able to predict what happens over a short time, but that over a longer time prediction is next to impossible [1,7].

3. Chaotic behaviour is constrained to a relatively narrow range. In other words, chaotic signals are bounded, implying, that although they appear random, on successive iterations the state/behaviour of the system stays within a finite range.

4. Chaotic behaviour has a definite form. There is a particular pattern to the behaviour. These patterns often take the form of bands – regions where behaviour preferentially occurs - and forbidden zones – regions where it does not exist – [1].

Chapter 3

Origin of the Heart Rate Variability Signal

3.1 Physiological Background

3.1.1 Anatomy

The heart is a prolate spheroid shaped, muscular organ lying obliquely in the thoracic cavity. The human heart is divided longitudinally by a partition into two halves between which there is no direct communication. The cavity of each side is further divided horizontally by an incomplete partition, which results in the formation of:

Two upper chambers: the right and left atrium

Two lower chambers: the right and left ventricles

The right atrium receives venous blood from the whole body and pumps it to the right ventricle. The latter pumps the blood to the lungs for reoxygenation. The oxygenated blood returns to the left atrium by the pulmonary veins, where it is delivered to the left ventricle. The left ventricle in turn, pumps this blood with sufficient pressure to reach all parts of the human body.

The heart muscle (myocardium) provides the main cardiac functions. Its rhythmic contractions provide the pumping force which contributes to the circulation. The myocardium has three physiologic properties: automaticity (the ability to initiate an

electrical impulse), excitability (the ability to respond to an electrical impulse), conductivity (the ability to transmit an electric impulse from one cell to another). It is formed of involuntary but striated muscles which branch and fuse with each other. The muscle fibers of the atria are continuous and behave as a single mass, similarly, are those of the ventricles. This arrangement allows electrical impulses necessary for contraction to spread very quickly. Two small masses of specialized tissue lie within the atrial myocardium:

(1). The sino-atrial (SA) node is located in the upper part of the right atrium. It is responsible for the initiation of impulses necessary for rhythmic heartbeats.

(2). The atrioventricular (AV) node is located in the lower part of the interatrial septum. It is responsible for conduction of impulses from the atria to the ventricles.

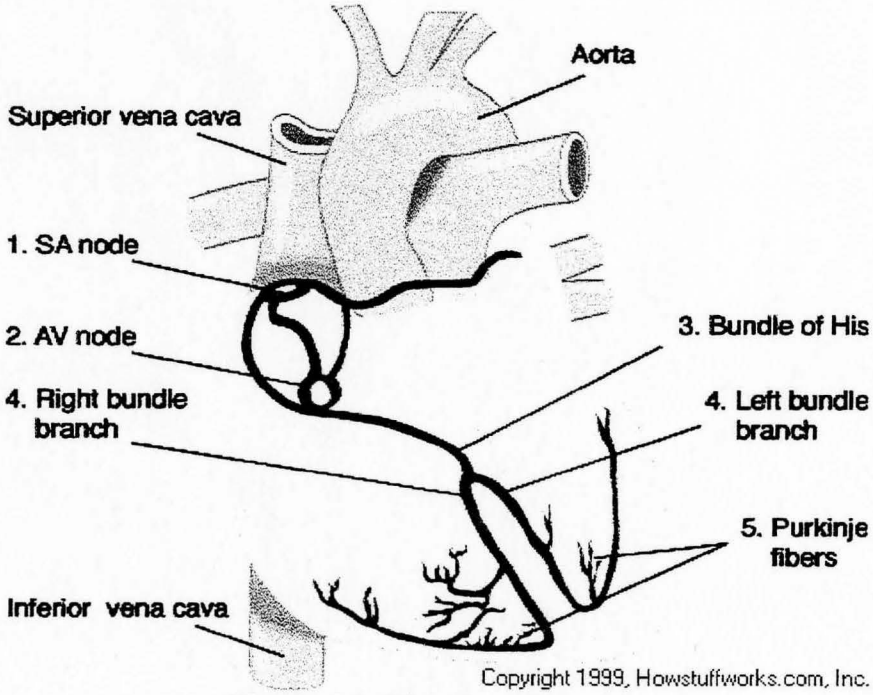

Figure 3.1: The Heart Structure

A bundle of fibers "the bundle of His" arises from the AV node and runs in the interventricular septum, where it divides into two branches the left and right bundle branches to supply each ventricle. Each bundle further divides into a fine network of fibers "The Purkinje fibers" which supply the ventricular myocardial cells. Cells of the SA node and AV node are specialized in initiating electrical impulses which are responsible for normal regular cardiac functions [10].

Occasionally, under special circumstances the heartbeat may originate in a region of the myocardium other than the SA node. These sites are termed ectopic pacemakers and the beats are labeled as ectopic beats. Ectopic beats are often premature and are followed by a compensatory pause (Kamath et al. 1996) [9].

3.1.2 Regulation of the cardiac activity

Under normal physiological conditions the heart rate is subject to both autonomic neural and humoral regulation (Braunwald 1992; Guyton & Hall 1996). The anatomical origins of the autonomic innervations of the heart are illustrated in Figure 3.2 [9].

Although the cardiac muscles are capable of generating their own impulses, nerve impulses from the parasympathetic and sympathetic divisions of the autonomic nervous system can modify and regulate these activities. Sympathetic neurons spread throughout the myocardium, innervating the SA and AV nodes as well as the atrial and ventricular myocardium. On the other hand, the parasympathetic impulses, which reach the heart via the vagus nerve, predominantly supply the SA and AV nodes, and to a lesser extent the atrial myocardium. At rest, the activity of the parasympathetic system predominates. In

general, sympathetic cardiac stimulation serves to increase the heart rate while parasympathetic input has the opposite effect [8,9,10].

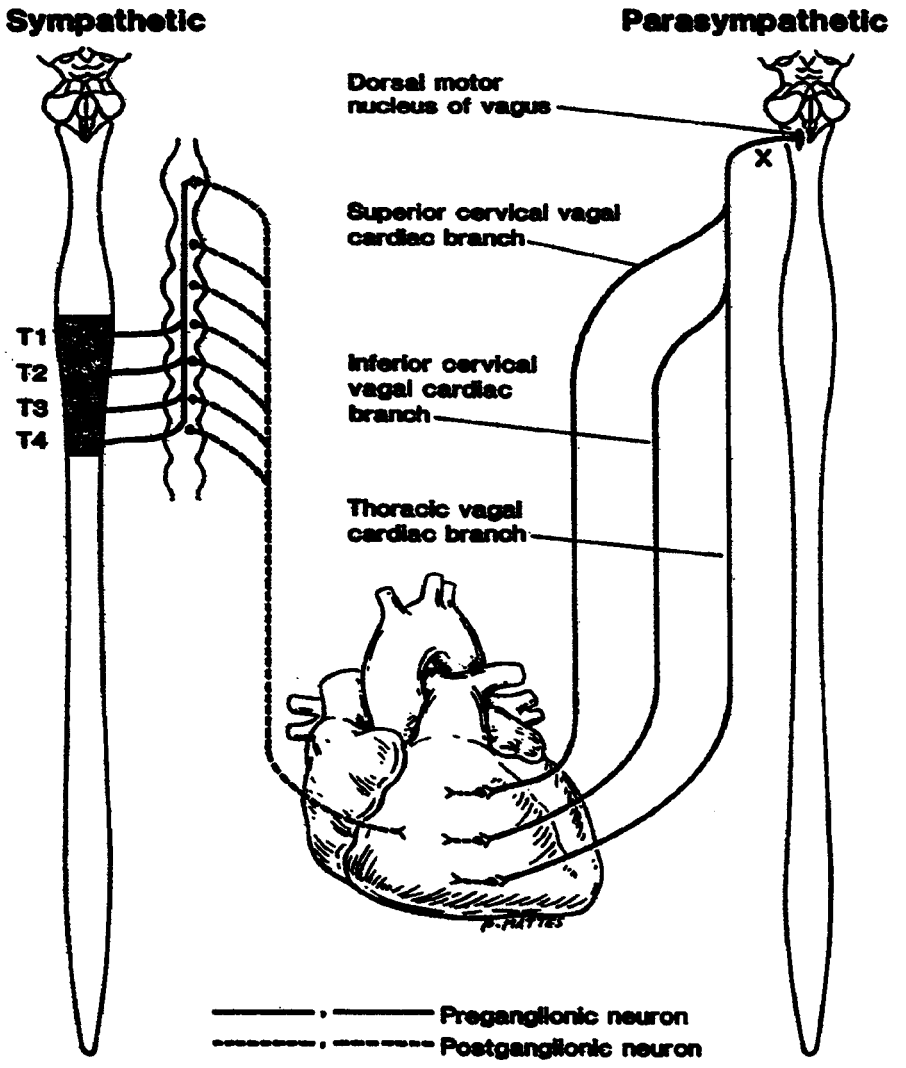

Figure 3.2: Diagram depicts nerve supply to the heart from both branches of the autonomic nervous system. Preganglionic fibers from both branches are represented by solid lines. Postganglionic fibers from both branches are represented by dashed lines: terminals from the sympathetic branch are distributed to the pacemaker, conduction system, atrial and ventricular myocardium, and coronary vessels; and from the parasympathetic branch fibers terminate in the sinoatrial and atrioventricular nodes, atrial and ventricular musculature, and coronary vessels. (From Hockman C H, *Essentials of autonomic function*. Springfield IL, pp.42, 1987).

3.1.3 The electrocardiogram (ECG):

Electrocardiography is the study of the electric activity associated with heart contraction. Each cardiac contraction results from electric currents, which spread from within the heart and can be monitored from the surface of the body. These currents, which reflect the electrical activity of the heart, are detected when electrodes are placed on the external surface of the body. The first ECG recordings were reported by Einthoven in 1912 [10]. ECG signal is the most easily observable signal from the human heart and as such has been subject to intensive analysis with regard to their significance in the context of pathologies. The recorded differences in electric potentials have a specific pattern in the cardiac cycle, each part of which represents the electric activity of a specific part of the heart:

1. SA Node
2. Atrial Muscle
3. AV Node
4. Atrioventricular Bundle
5. Left and Right Bundle Branches

Traditionally the ECG cycle is labeled using the letters P, Q, R, S, T for the individual peaks of the cycle's waveform:

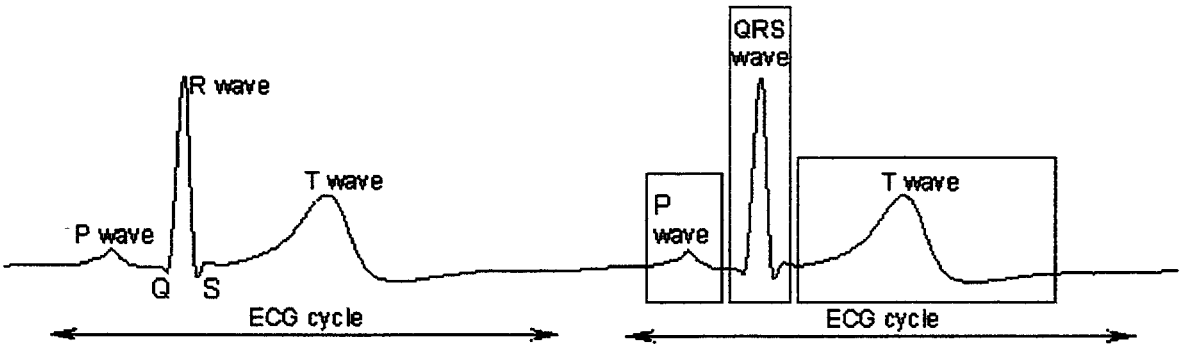

Figure 3.3: QRS Complex

P = atrial wave.

QRS = wave of rapid ventricular depolarization < 0.1 sec.

T = wave of ventricular repolarization.

3.2 The Heart Rate Variability Signal

HRV refers to the changes in the length of time between consecutive heartbeats. A heartbeat is usually measured as the time (in msecs) from the peak of one R wave to the peak of the next. This time is referred to as the *RR interval*. Under resting conditions, the ECG of healthy individuals exhibits periodic variation in R-R intervals. Part of this rhythmic phenomenon, known as respiratory sinus arrhythmia (RSA), fluctuates with the phase of respiration -- cardio-acceleration during inspiration, and cardio-deceleration during expiration. RSA is predominantly mediated by respiratory gating of parasympathetic efferent activity to the heart: vagal efferent traffic to the sinus node occurs primarily in phase with expiration and is attenuated during inspiration.

Reduced HRV has thus been used as a marker of reduced vagal activity. However, because HRV is a cardiac measure derived from the ECG, it is not possible to distinguish reduced *central* vagal activity (in the vagal centers of the brain) from reduced peripheral activity (the contribution of the target organ -- the sinus node or the afferent/efferent pathways conducting the neural impulses to/from the brain). The analysis of HRV offers a non-invasive method of evaluating vagal input into cardiac rhythm.

Chapter 4

Chaos in Physiology and effects of Aging on the Heart Rate Variability Signal

4.1 Introduction

Constant internal environment within the human body, more commonly known as 'homeostasis' is a result of multiple control systems and enables an individual to adapt to the external environment continuously. However, the internal milieu responds to the demands placed on it by external variables through both linear and nonlinear mechanisms. Therefore, the system may include both linear and nonlinear components. As human subjects age, it is hypothesized that there is a loss of dynamic range in the physiologic function with the resulting inability to adapt to stressful situations [20]. Such loss of dynamics is likely due to a loss of complexity of the organ or the function being measured. The concept that deterministic chaos is present in the physiological systems has been a major issue concerning researchers for the past several years. There is no direct evidence that the body operates strictly according the rules and algorithms of a nonlinear dynamical system. However, over the years, scientists have presented anecdotal observations and more recently, substantive evidence to support the hypothesis that characterizing a physiological system through nonlinear mathematical methods may provide a better representation of the underlying processes and permit us to understand

pathological conditions or effects of pharmacological and/or other therapeutic interventions.

4.2 Evidence for the Presence of Chaos in Physiological Signals

Nonlinear behaviour was first identified in cardiac tissue by Guevara et al. [11], and subsequently by Chialvi and Jalife [12] with similar results. Various researchers like Ritzenberg et al. [13], Chen et al. [14], Goldberger et al. [15], Shrier et al. [16], and Winfree et al. [17] examined various aspects of this hypothesis thereby demonstrating the power of applying principles of mathematical analysis (nonlinear dynamics) to cardiac physiology.

While inter-individual measures of aging may be based on specific physiological experiments (e.g.: measurements on nerve conduction velocity, insulin sensitivity), it is likely that mathematical abstractions based on nonlinear dynamics may help us to quantify the aging process and pathological conditions more accurately. For example, there is a loss of high frequency waves in the EEG with age [41]. This loss of dynamic frequency range is attributed to a loss of neuron number, impaired cerebral energy metabolism, reduced cerebral perfusion and disrupted internal connections [42]. A loss of complexity in the regulation of anterior pituitary hormone secretion is also apparent with aging in humans. Pulsatile release of growth hormone, leuteinizing hormone, and thyrotropin are attenuated with aging. The standard deviation of the mean interval between thyrotropin pulses is smaller in healthy elderly subjects compared with healthy young subjects, suggesting a less complex pattern of hormonal secretion with aging [47, 49].

While the field of identifying deterministic chaos in physiology is in infancy and the evidence is still being sought by various laboratories, it is of interest to ask, as to where the observed chaotic behaviour originates. This leads one to the following questions:

a) Is the presence of nonlinear dynamical behaviour determined by the anatomical structure of the organs whose function we attempt to model?

b) Do the brain and the central nervous system have a role to play in generating the observed chaotic signal?

A promising advance in the contemporary understanding and quantification of healthy variability has been the introduction of fractal mathematics to study biological systems. The term fractal describes a wide class of complex shapes and processes in nature. Fractal shapes are irregular and have non-integer or fractional, dimensions. Unlike a smooth Euclidean line, a fractal line, which has a dimension between 1 and 2, is wrinkly and irregular. Examining these wrinkles closer, results in smaller wrinkles on the larger ones. Further magnification shows yet smaller wrinkles, and so on. A fractal is an object composed of subunits, and sub-subunits that resemble the larger scale structure, a property known as self-similarity [18].

Fractal processes generate irregular fluctuations on multiple time scales. Furthermore, such temporal variability is statistically self-similar. Qualitative appreciation for the self-similar nature of such fractal processes can be obtained by plotting the time series in question at different magnifications, as shown in Figure 4.1 [18].

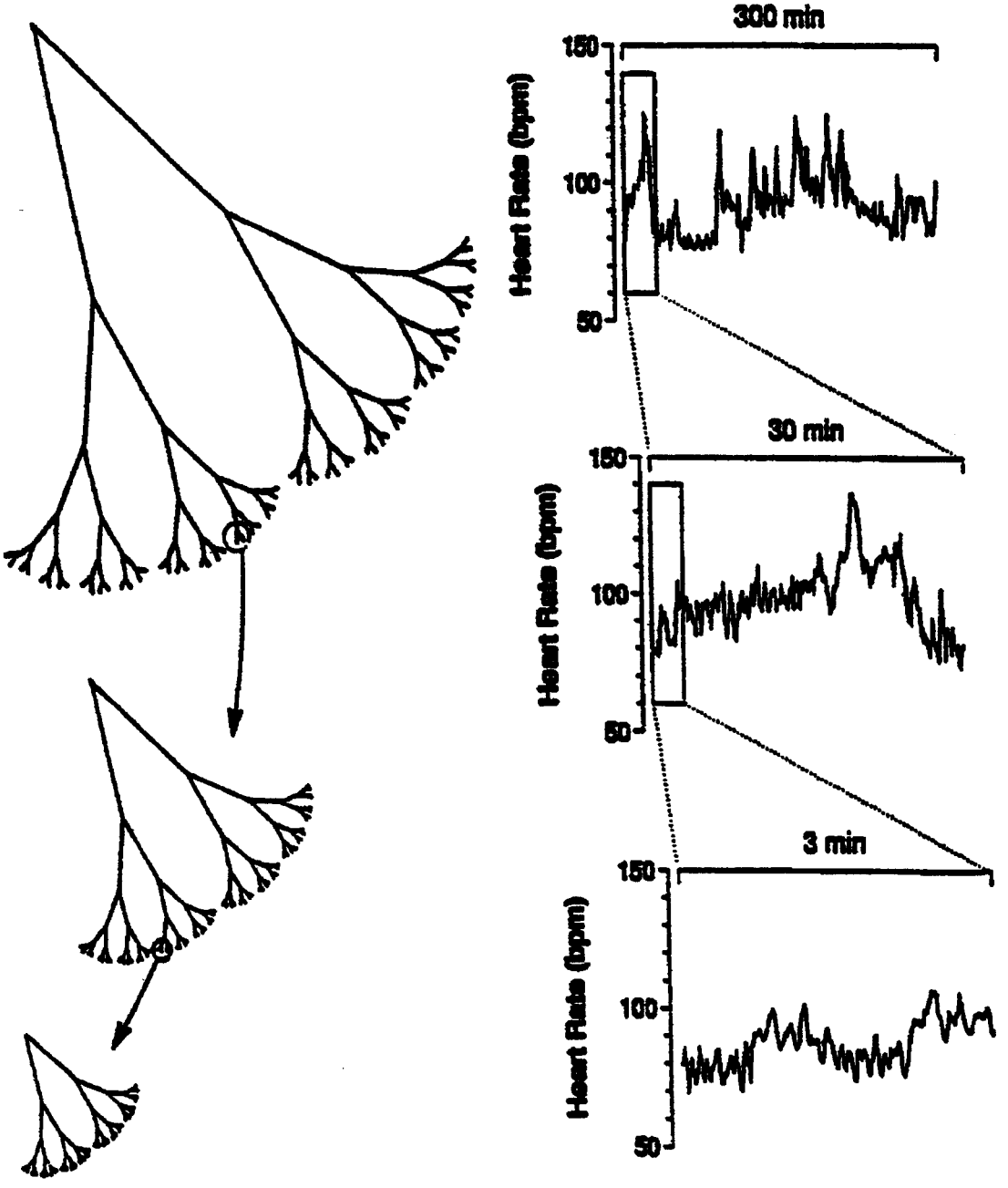

Figure 4.1: A fractal object, like a tree (left) has self-similar branching such that the small-scale structure when magnified resembles the larger scale form. A fractal process, such as heart rate regulation (right), generates irregular fluctuations on different time scales that are statistically self-similar. It should be noted that while idealized fractals may be constructed with identical subunits, fractal objects are usually asymmetric and irregular. (From [18]).

Goldberger and his colleagues have argued in a number of publications that the self-similar structure within the anatomy of certain organs contributes to the genesis of chaotic behaviour [18]. For example, the bronchial tree has self-similar branches. Also in a myocardium, the fractal-like conduction tree is asymmetric and irregular, and therefore the arrival times of these electrical impulses in the myocardium will be decorrelated, and may give rise to non-linear signals [19]. While the above argument is plausible, concrete scientific evidence (anatomic or otherwise) supporting the complexity hypothesis in physiology is still elusive. Regarding the role of the central nervous system in generating the chaotic signals waveforms, a stronger case may be made regarding the characteristics of the basic elements of the CNS, which contribute to the origin of the signals. It is well established that the individual neurons are nonlinear elements and act in a binary fashion. Therefore, it is not inconceivable that an organ (brain) made of non-linear elements (i.e. neurons) can give rise to non-linear properties at a macro-level and give out signals which may have a non-linear dynamic behaviour.

4.3 HRV Signal and the Effect of Age

While discrete impulses to generate the ECG signal originates in the sino-atrial node, regulation of the heart beat intervals on a beat-by-beat basis is under central command located within the mid-brain structures. For more than 20 years, analysis of the HR signal through time domain and frequency domain indices provided a number of insights into the modulatory mechanisms that determine the cardiovascular function. Recent addition of nonlinear indices to study the heart rate variability has enabled a study

of number of issues regarding the autonomic control of hemodynamic signals including effects of aging.

Literature on effects of aging on the autonomic function is vast and is spread among a number of journals in physiology, clinical medicine, cardiology and gerontology. We therefore, present a selected review of literature on both linear and nonlinear analysis of the HRV signal and which examines the effects of age. Since linear analysis has been around longer, several investigators have contributed to the literature on the subject. Only a handful of groups have evaluated the changes in non-linear indices with respect to age [20, 23, 43, 42].

Ryan et al. analyzed heart rate dynamics during 8-minute segments of ECG in 40 men and 27 women of various ages while they performed spontaneous and metronomic breathing. This study attempts to quantify complex dynamics of beat-to-beat heart rate fluctuations and determine if complexity differs with gender and age [44]. Power spectral analysis and approximate entropy were computed. It was found that high frequency power and the ratio of high/low frequency power within the HRV signal decreased with age. The high/low frequency power ratio during spontaneous and metronomic breathing was greater in women than men. Approximate entropy of the heart rate decreased with age and was higher in women than men.

Fluckiger et al. [48] studied the differential effects of aging on heart rate variability and blood pressure variability in 65 healthy subjects aged between 18-80 years. Their results suggest that there is a continuous decline with age of normalized LF power in the standing position and the normalized spectral power of HR during paced

breathing. Fluckiger et al. conclude that effect of aging on the ANS is progressive and continuous throughout the age groups studied. Although aging process diminished HR variability and diastolic BP variability, it had no influence on the systolic blood pressure variability.

Yamasaki et al. [45] evaluated the diurnal HRV in 105 healthy subjects (ages: 20-78 years, 63 males and 42 females) using Holter recorded ECG and power spectral analysis of the HRV signals. The investigators also examined the effects of gender on the effects of aging. It was noted that male subjects had consistently higher low frequency power and it correlated with age. The investigators conclude that sympathetic function is pronounced with age in younger healthy male subjects and that sympathetic function declines more linearly than parasympathetic function. Also, parasympathetic function is better retained in older females compared to older males.

Sakata et al. [46] studied 62 healthy men aged 21-79 years in their laboratory to evaluate the effects of aging on the HRV. They studied log-log scaled spectra computed from 24- hour HRV signal. Authors state that there may be two independent contributors to the power spectral components which influence their decay with frequency, one determined by the age and the second determined by the dynamics of the individual.

Pikkujamsa et al. [23] studied the effects of age on R-R intervals. ECG recorded on a 24 hour Holter from 114 healthy subjects (age: 1-82 years) was analyzed using time domain, frequency domain and nonlinear dynamical (chaos) indices. Investigators conclude that cardiac interbeat interval dynamics change markedly from childhood to old age in healthy subjects with a loss of complexity with age.

Spectral analysis alone, a technique based on linear mathematics, is of limited value while assessing the complexity of nonlinear systems. The aging process in the absence of disease, appears to be marked by a progressive impairment in multiple control mechanisms that enable an individual to adapt to the unpredictable changes of everyday life, resulting in loss of dynamic range in physiologic function. This hypothesis, relating aging to loss of complexity suggests new ways to monitor the physiologic aging process based on nonlinear measurements [20]. These methods will be discussed in the next chapter.

4.4 Conclusion

Evidence for chaos in physiological signals is slowly emerging. However, an understanding of physiological mechanisms that are responsible for the genesis of deterministic chaos is still being developed. We have reviewed some relevant literature to support the hypothesis that deterministic chaos may be present in the heart rate variability signal. It is generally believed that aging reduces the complexity of the heart rate variability signal.

Chapter 5

Indices of Nonlinear Dynamics of the HRV Signal

5.1 Introduction

In this chapter, we will study and evaluate nonlinear indices that can be applied to test the hypothesis that deterministic chaos may be present in the heart rate variability signal and that aging may reduce the complexity of the signal.

5.2 Power-Law Scaling

The recent observation that heart rate variability demonstrates self-similarity across multiple orders of temporal magnitude, suggests that the mechanisms underlying heart rate regulation may have fractal properties [3].

Increasing attention is being focused on quantifying various aspects of heart rate dynamics associated with beat-to-beat fluctuations due to limited information about autonomic control of heart rate obtained by traditional measures. Spectral analysis is a useful technique for quantifying the overall heart rate variability. Specific components of this variability are associated with respiration, sympathetic nervous system activity and other physiological influences. Spectral analysis transforms the HRV signal into its constituent frequency components and quantifies the relative power (squared amplitude) of these components [21].

Spectral analysis of HRV is characterized, in addition to very low frequency components (0 to 0.03 Hz), by 2 major oscillatory components at low frequency (LF~0.1 Hz) and high (HF~0.25 Hz) frequency. The low frequency component at 0.1Hz, is used as an indirect index of sympathetic modulation, whereas the higher frequency component at 0.25Hz is used as an index of vagal modulation. Both LF and HF components account for up to 65% of total power when short-term recordings are considered [22].

To quantify the dynamic differences in the inter-beat interval time series, standard fast Fourier transform methods are applied to derive the power spectral density estimates of 20-minutes of the HRV signal. A presentation in a log-log plot demonstrates a decaying curve, in which the power is inversely proportional to the frequency ($1/f^{\beta}$) in a range between 10^{-3} to 10^{-1} (the interval that most corresponds to very low (<0.01) and low frequency range (0.1Hz)). The exponent β in this power-law relationship between frequency and power is called scaling exponent β. This exponent is calculated by a regression analysis of log(power) and log(frequency) plots of the smoothed power spectrum over the frequency range of 10^{-3} to 10^{-1} Hz. The value β of the exponent measures the degree of signal correspondence to a power-law process, a value of 0 represents the flat spectrum of white noise, whereas other values suggest that there are correlations in the data [4,5,23,24]. For healthy control subjects, β ranges between –1.18 (for pediatric subjects) to –1.38 (for elderly subjects) [23].

Recent analysis of cardiac beat-to-beat intervals in healthy subjects over long time intervals, show scale-invariant long-range correlations. In subjects with severe heart disease, the distribution of heartbeat intervals is unchanged, but long-range correlations

are either diminished or lost. The $1/f$ nature of heart rate variability is rather poorly understood, but may be related to the interaction of multiple physiological control systems that operate over many different time scales. The regulation of the heart rate over multiple time scales may serve to broaden the frequency response of the cardiovascular system and permit it to adapt to an unpredictable and changing environment. The breakdown of such long-range correlations may be associated with the development of disease states and an associated loss of adaptive capacity [3].

Physiological aging is associated with a reduction in parasympathetic control of heart rate. Because we hypothesize that there is selectively greater loss of high-frequency heart rate variability in older than in younger subjects, we anticipate a more negative slope for older subjects, that is, β would be greater in the older subjects when compared to those of pediatric, young adult and middle aged subjects [21].

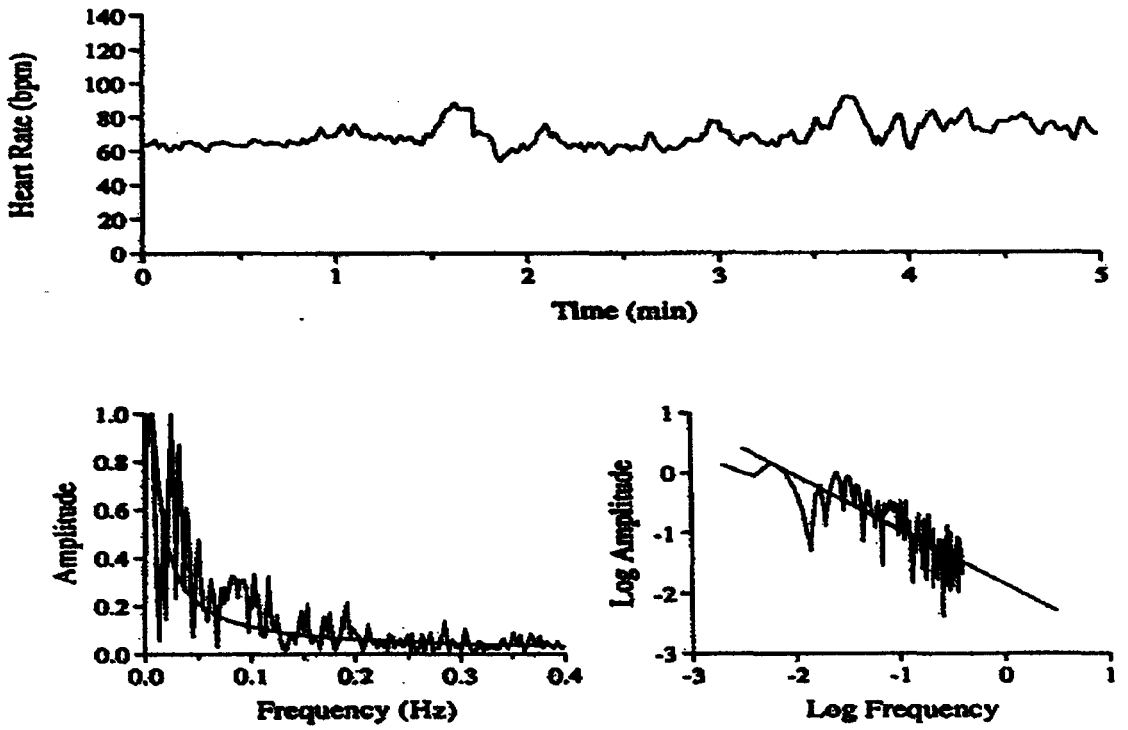

Figure 5.1: Heart rate dynamics in the supine position are analyzed in 3 steps. *Top*: First, Heart rate is computed from the RR-interval vs. beat number to obtain HR vs. time. *Bottom left*: Second, with a fast Fourier transform, the heart rate frequency is computed for the heart rate time series. *Bottom right*: last, the HR spectrum is replotted on double-log axes (log amplitude vs. log frequency), and a regression line is fit to the data points. This regression gives a $1/f^{\beta}$ plot (From [21]).

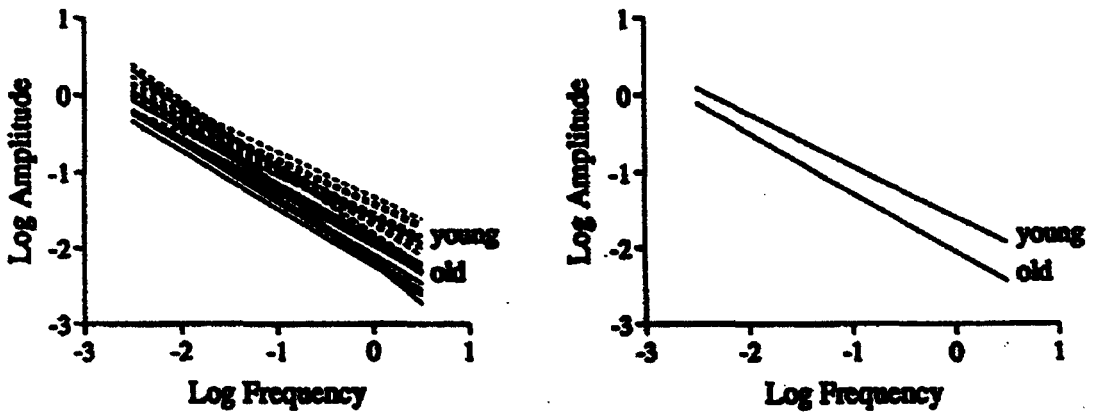

Figure 5.2: Heart rate spectral distribution for young and old subjects, quantified by log amplitude versus log frequency ($1/f^{\beta}$) plots. *Left*: individual $1/f^{\beta}$ regression lines for each subject. *Right*: average regression lines for young and old subjects (From [3]).

5.3 Approximate Entropy

Approximate entropy (ApEn), has been recently introduced to quantify of regularity in time-series data, motivated by applications to relatively short length (20 minutes – 1 hour) HRV signal available in human subjects. Research using ApEn helped to discriminated groups of subjects, in instances where classical [mean, standard deviation] statistics did not show clear group distinctions [30].

ApEn quantifies the predictability of fluctuations in a given time domain signal such as the heart rate. Intuitively, one may reason that the presence of repetitive patterns of fluctuation in a time series renders it more predictable than a time series in which such patterns are absent. ApEn measures the (logarithmic) likelihood that data points a certain distance apart ($\boldsymbol{r}$) for a given number ($\boldsymbol{m}$) of observations will remain within the same distance on the next incremental comparisons. A greater likelihood of remaining the same distance apart, i.e., a greater regularity or predictability, produces lower ApEn values. On the other hand, the more complex (less predictable) the process generating the HRV signal, the higher the ApEn value [29, 31].

Investigators [31, 32, 34] have associated sickness and aging with significantly decreased ApEn values, consistent with the hypothesis associating compromised physiology with more regular, patterned sinus rhythm HR tracings, and normative physiology with greater irregularity (randomness, more complexity).

Two input parameters, $\boldsymbol{m}$ and $\boldsymbol{r}$, must be fixed to compute ApEn: $\boldsymbol{m}$ is the "length" of compared runs, and $\boldsymbol{r}$ is effectively a filter. Given N data points $\{u(i)\}$, form vector sequences $\mathbf{x}(1)$ through $\mathbf{x}(N - \boldsymbol{m} + 1)$, defined by $\mathbf{x}(i) = [u(i),\ldots,u(i + \boldsymbol{m} - 1)]$. These

vectors represent $\boldsymbol{m}$ consecutive u values, commencing with the ith point. Define the distance $d[\mathbf{x}(i), \mathbf{x}(j)]$ between vectors $\mathbf{x}(i)$ and $\mathbf{x}(j)$ as the maximum difference in their respective scalar components. Use the sequence $\mathbf{x}(1), \mathbf{x}(2),\ldots\ldots,\mathbf{x}(N-\boldsymbol{m}+1)$ to construct, for each $i \leq N-\boldsymbol{m}+1$:

$$C_i^m(\boldsymbol{r}) = (\text{ no. of } j \leq N-\boldsymbol{m}+1 \text{ such that } d[\mathbf{x}(i), \mathbf{x}(j)] \leq \boldsymbol{r})/N-\boldsymbol{m}+1.$$

The $C_i^m(\boldsymbol{r})$ values measure within a tolerance $\boldsymbol{r}$ the regularity, or frequency, of patterns similar to a given pattern of window length $\boldsymbol{m}$. Define:

$$\Phi^m(\boldsymbol{r}) = (N-\boldsymbol{m}+1)^{-1} \sum_{i=1}^{N-m+1} \ln C_i^m(r)$$

where ln is the natural logarithm, and then define the parameter ApEn (m, r) = $\lim_{N\to\infty}$ $[\Phi^m(\boldsymbol{r}) - \Phi^{m+1}(\boldsymbol{r})]$. Given N data points, we estimate this parameter by defining the statistic ApEn $(\boldsymbol{m}, \boldsymbol{r}, N) = \Phi^m(\boldsymbol{r}) - \Phi^{m+1}(\boldsymbol{r})$ [32, 33, 34, 35]. On unraveling definitions the following essential observation is deduced:

-ApEn = $\Phi^{m+1}(\boldsymbol{r}) - \Phi^m(\boldsymbol{r})$ = average over i of ln [conditional probability that $|u(j+\boldsymbol{m}) - u(i+\boldsymbol{m})| \leq \boldsymbol{r}$, given that $|u(j+\boldsymbol{k}) - u(i+\boldsymbol{k})| \leq \boldsymbol{r}$ for $\boldsymbol{k} = 0, 1,\ldots, m-1$]

The flow here is that given a time series of N data points, we form an associated time series of $N-\boldsymbol{m}+1$ vectors, each vector consisting of $\boldsymbol{m}$ consecutive points. For example, with $\boldsymbol{m}=2$ here, the first three vectors are $[u(1), u(2)]$, $[u(2), u(3)]$, and $[u(3), u(4)]$. Each vector serves, in turn, as a template vector for comparison with all other vectors in the time series, toward the determination of a conditional probability associated with this vector. The conditional probability calculation consists of first obtaining a set of conditioning vectors close to the template vector and then determining

the fraction of instances in which the next point after the conditioning vector is close to the value of the point after the template vector. Finally, ApEn aggregates these conditional probabilities into an ensemble measure of regularity [32, 33].

There are two important issues while applying ApEn to experimental data: computational demands and noise effects. These issues determine the fixed values required as input parameters of ApEn, $\boldsymbol{m}$ and $\boldsymbol{r}$ [34]. These choices of $\boldsymbol{m}$ and $\boldsymbol{r}$ are made to ensure that the conditional probabilities are reasonably estimated from the N input data points. Theoretical calculations indicate that reasonable estimates of these probabilities are achieved with an N value from 10^m to 30^m data points, analogous to a result for correlation dimension reported by Wolf et al. [ref]. For $\boldsymbol{r}$ values smaller than 0.1 SD, one usually achieves poor conditional probability estimates as well, whereas for $\boldsymbol{r}$ values larger than 0.25 SD, too much detailed system information is lost [ref]. Therefore, it has been concluded that for $\boldsymbol{m} = 2$ and $N = 1024$, values of $\boldsymbol{r}$ from 0.1 to 0.25 SD of the $u(i)$ data produce good statistical validity of ApEn($\boldsymbol{m}$, $\boldsymbol{r}$, N) for many models [32, 33, 35].

5.4 Detrended Fluctuation Analysis (DFA)

The technique of detrended fluctuation analysis (DFA) was recently introduced, based on a modified root-mean-square analysis of a random walk, to assess the intrinsic correlation properties of a dynamic system separated from external trends in the signal [24]. DFA quantifies fractal-like correlation properties of a time domain signal. The root-mean-square fluctuation of the integrated and detrended signal are measured in observation windows of various sizes and then plotted against the size of the window on a log-log scale. The scaling exponent $\boldsymbol{\alpha}$ represents the slope of this line, which relates

(log) fluctuation to (log) window size. Two scaling exponents are calculated: α_1, the short-term exponent (4 to 11 beats), and α_2, the intermediate-term exponent (>11 beats). In this study, the scaling exponents were calculated from segments of 1024 beats of supine ECG recording, and 8192 beats from 24-hour holter ECG recording [4, 23].

The DFA is used as a measure of the correlation properties of a signal. This method permits the detection of correlations embedded in a seemingly nonstationary signal and avoids the spurious detection of apparent long-range correlations that are due to artifacts (i.e. nonstationarity). Because the detrending procedure is implemented on all scales, DFA can be used to quantify the self-similar properties of a signal [24, 26].

To illustrate the DFA algorithm, we use the interbeat R-R interval signal shown in Figure 5.3, as an example. The total length of the interbeat (i.e. R-R) interval time series (N) is first integrated as follows:

$$y(k) = \sum_{i=1}^{k} \left[RR(i) - RR_{avg} \right] \tag{5.1}$$

where $RR(i)$ is the ith interbeat interval and RR_{avg} is the average interbeat interval. Next, the integral time series is divided into boxes of equal length n (Figure 5.3 c). In each box of length n, a least-squares line is fitted to the data (representing the trend in that box) Figure 5.3. The y-coordinate of the straight-line segments is denoted by $y_n(k)$. Next, we detrend the integrated time series, $y(k)$, by subtracting the local trend, $y_n(k)$, in each box. The root-mean-square fluctuation of this integrated and detrended time series is calculated by

$$F(n) = \sqrt{1/N \sum_{k=1}^{N} \left[y(k) - y_n(k) \right]^2} \tag{5.2}$$

This computation is repeated over all time scales (box sizes) to provide a relationship between $F(n)$, the average fluctuation as a function of box size, and the box size n (Figure 5.3 c). Typically, $F(n)$ will increase with box size (Figure 5.3 d). A linear relationship on a double-log graph indicates the presence of scaling, i.e., $F(n) \approx n^{\alpha}$. Under such conditions, the fluctuation can be characterized by a scaling exponent α, the slope of the line relating log $F(n)$ to log n. An α of 0.5 corresponds to white noise, $\alpha = 1$ represents $1/f$ noise, and $\alpha = 1{,}5$ indicates Brownian noise or random walk. The exponent α is related to β by a simple formula: $\beta = 1 - 2\alpha$ [24, 26, 27]. This relationship is valid at the infinite length limit. For time series with finite length, it is expected that discrepancies occur between β and α [25].

A good linear fit of the log $F(n)$ vs. log n plot indicates that $F(n)$ is proportional to n^{α}, where α is the single exponent describing the correlation properties of the entire range of time scales. However, the observation that the DFA plot was not strictly linear but rather consisted of two distinct linear regions of different slopes separated at a break point suggests there is short-range scaling exponent, α_1, over periods of 4 to 11 beats, and a long-range exponent, α_2, over long periods [5].

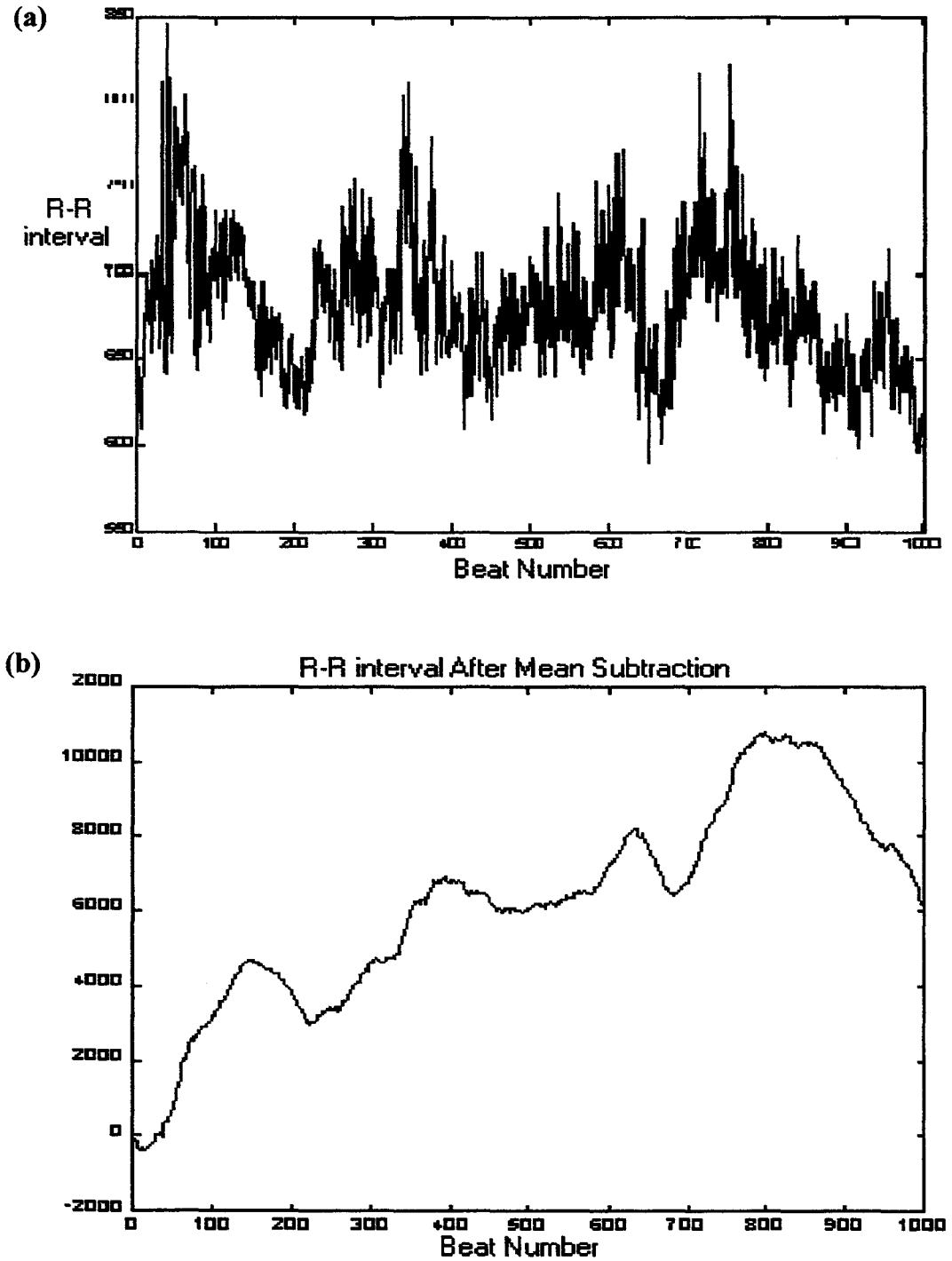

Figure 5.3: DFA of the R-R interval. (**a**) R-R interval of a subject, (**b**) R-R interval after equation 5.1,

(c)

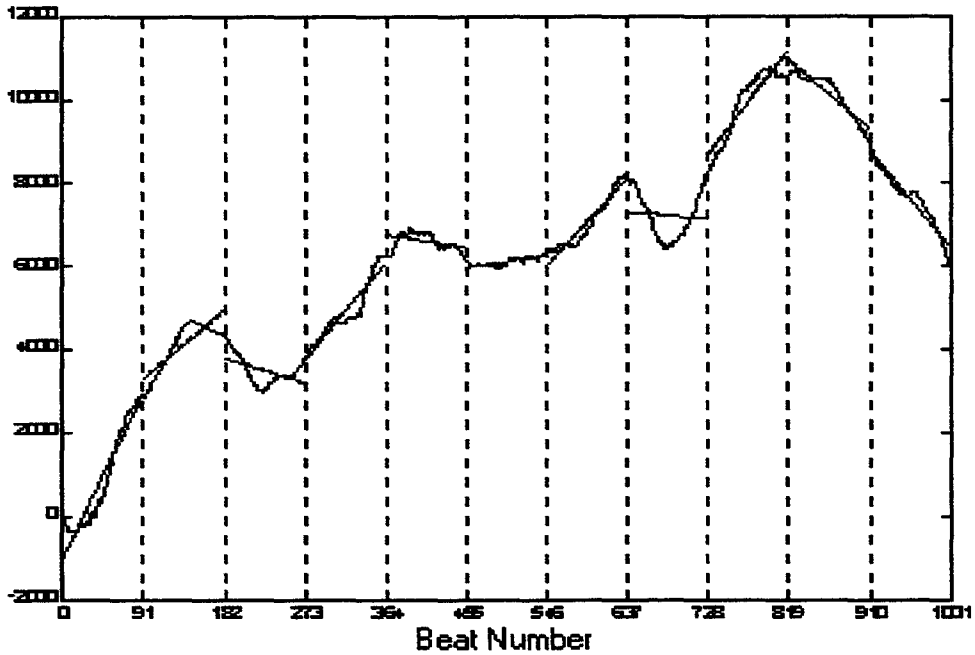

(d)

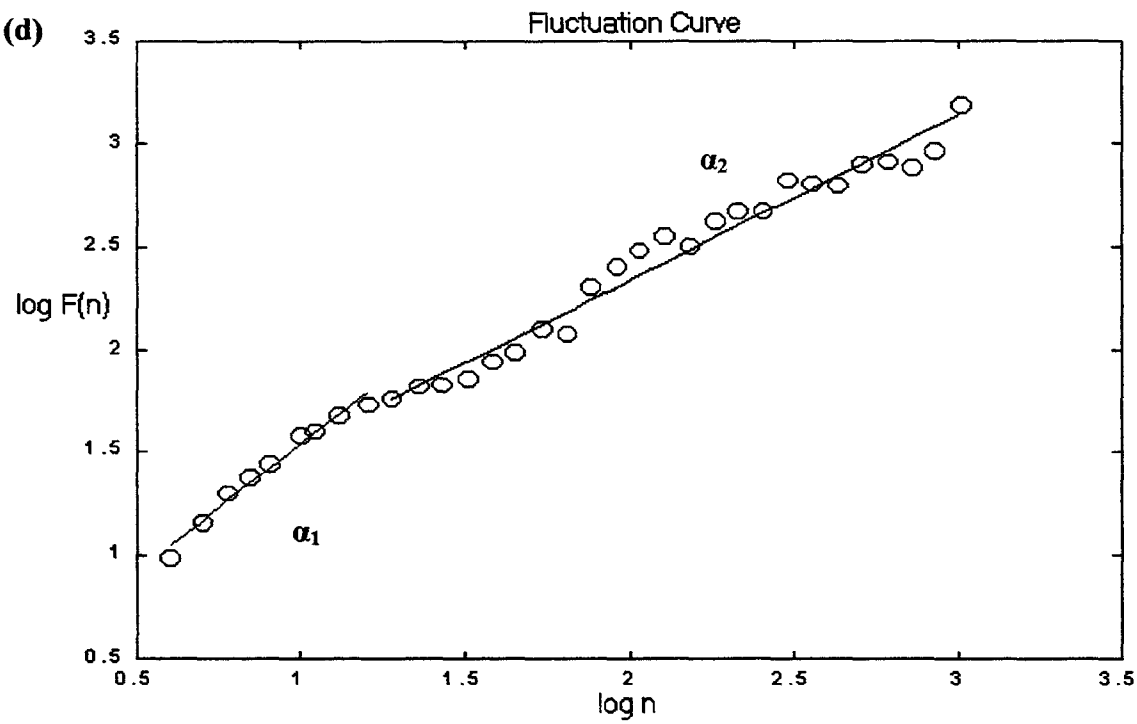

Figure 5.3: DFA of the R-R interval. **(c)** n windows, and each window has a linear regression line fitting its data, **(d)** the fluctuation curve, log $F(n)$ vs. log n shows the two scaling exponents, α_1 short-range and α_2 long-range.

5.5 Correlation Dimension and Surrogate Data

The null hypothesis that the HRV signal is generated by a linear stochastic process is tested using the following indices: a discriminating statistic representing the measured signal is derived. Often, the discriminating statistic is some parameter that can be computed from the measured time series (signal) and also from a time series that is consistent with the null hypothesis (i.e. surrogate data sets). In this study, the correlation dimension $\boldsymbol{D}$ is used as the discriminating statistic.

We test if the measured HRV signal is consistent with the null hypothesis in the following way: First, calculate the value of the discriminating statistic from the HRV (the value of $\boldsymbol{D}$). Then find the range of values of the discriminating statistic for a generated time series that is consistent with the null hypothesis. If $\boldsymbol{D}$ falls within this range of values, then the discriminating statistic cannot distinguish between the null hypothesis and the HRV signal. On the other hand, if $\boldsymbol{D}$ falls outside this range, then the HRV signal is inconsistent with the null hypothesis [7].

5.5.1 Surrogate data analysis

One way of finding the range of values of the discriminating statistic for a time series (signal) consistent with the null hypothesis is to generate many different time series that are consistent with the null hypothesis, and then calculate the value for the discriminating statistic for each these time series. Such data that are generated to be consistent with the null hypothesis are called **surrogate data sets** [7].

The method of surrogate data analysis was originally developed by Theiler et al. [51] to detect any nonlinearity present in the time series. Since nonlinearity is the

essential criteria for chaotic dynamics, the technique is widely applied [52, 53, 54] to rule out the presence of linear stochastic processes in an observed time series. In this study, random phase surrogate sets are generated and used to test the null hypothesis that the HRV signal is generated by a linear stochastic process [50].

The generation of random phase surrogate data addresses to a hypothesis that the original HRV signal is linearly correlated Gaussian noise. This type of surrogates are generated by the following steps:

Step1: Compute the Fourier transform of the original HRV signal. This will consist of an amplitude $A(\omega)$ and a phase $\Phi(\omega)$ at each frequency ω.

Step2: Replace the phases $\Phi(\omega)$ with random numbers ranging between 0 and 2π. Note that this has no effect on the amplitude $A(\omega)$. (Note that in the original time series, $\Phi(\omega) = -\Phi(-\omega)$, and this symmetry should be maintained when assigning random phases.)

Step3: Compute the inverse Fourier transform of $A(\omega)$ and the randomized $\Phi(\omega)$. This produces a new signal, called the surrogate data.

The surrogate data has the same amplitude spectrum $A(\omega)$ as the original signal. Since the power spectrum is proportional to $A^2(\omega)$, the surrogate data time series has exactly the same power spectrum as the original signal [7, 50].

Because we want to find the range of values for the discriminating statistic for data consistent with the null hypothesis, we will want to make many different surrogate data time series. This is performed by applying the same process, however, using

different random numbers for the phases $\Phi(\omega)$ in step 2. Typically, 10 to 100 different surrogate data sets may be generated. In the present study, we use 10 randomly generated surrogate data sets. The above procedure of generating surrogate data is tested in the next chapter to show that the spectrum of a signal before and after phase randomization is identical.

5.5.2 Correlation dimension

To compare the original and the surrogate data sets, a discriminating statistic is calculated for both signals. As pointed out by Theiler et al. [51], in principle any statistics can be used for this purpose. We use the correlation dimension ***D*** as our discriminating statistic [56].

The correlation dimension ***D***, is one of the several types of dimensions in the dimension spectrum that characterizes the multifractal structure of the chaotic attractor. The Grassberger and Procaccia [57] algorithm with multivariate embedding is used to calculate the discriminating statistic in the present work [55].

For a time series of length N, the vector $x(i)$ is constructed where i= 1, 2, ..., N, and the coordinates of $x(i)$ are the sample values at time i. The correlation integral $C(r)$ represents the fraction of distances smaller than r. The Euclidean distance metric is used as a measure of distance. $C(r)$ is determined for a range of r-values (r_{min} to r_{max}) with

$$C(r) = \frac{2}{N(N-1)} \sum_{j=1}^{N-1} \sum_{i=j+1}^{N} \Theta(r - \| x_i - x_j \|) \tag{5.3}$$

Where $\Theta(\ )$ is the Heaviside function given by $\Theta(x) = 1$ for $x \geq 0$ and 0 otherwise, and the norm is defined by $\| x \| = \max\{| x_i |: 1 \leq i \leq m\}$.

When log $C(r)$ is plotted against log r, the correlation dimension $\boldsymbol{D}$ can be calculated from the line fitting this curve,

$$D = \min_{r \to 0} \frac{\log C(r)}{\log r} \tag{5.4}$$

This process is repeated for embedded dimension $m = 2$ to 20. To compare results at various embedded dimensions, we normalize the time series.

5.6 Conclusion

In this chapter, we discussed in details the five nonlinear indices applied to the HRV signal. These techniques may give us insight into the cardiovascular system.

Chapter 6

ECG and HRV Signal Acquisition and Processing

6.1 Introduction

In this chapter, we present details of acquisition of the ECG and the HRV signals for testing the hypothesis presented in earlier chapters. ECG data from 93 subjects was acquired for the present study and the corresponding HRV signal was computed. Details of recording conditions and preprocessing are also provided below.

6.2 Subjects –Recruitment & Screening

The ECG and the HRV signals analyzed in this research were obtained from a study of linear signal processing conducted in our laboratory [9]. A total of 93 healthy subjects (41 males and 52 females) ranging in age between 5 and 78 years volunteered to participate in this investigation. Subjects were from pediatric (PED, 5-12 years, n=15, 9 male, 6 female), adolescent (ADO, 13-17 years, n=16, 6 male, 10 female), adult (ADL, 18-30 years, n=22, 12 male, 10 female), middle aged (MDA, 31-60 years, n=21, 8 male, 13 female) and elderly (ELD, 61+ years, n=19, 6 male, 13 female) age groups. Subjects over the age of 55 years were recruited from the McMaster University Seniors Exercise Program. The remaining participants were recruited from the undergraduate/graduate student populations, faculty and staff at McMaster University or from local public schools.

Participants were initially contacted and interviewed by phone to provide information regarding the purpose and procedures involved in the study and to ensure that all general inclusion criteria were met. The investigation required that all subjects were healthy, non-smokers with no history of cardiovascular disease (including hypertension) or diabetes mellitus. The presence of any of the aforementioned conditions, a seated resting blood pressure over 160/95mmHg [36], or a BMI of greater than 25 kg/m^2 resulted in exclusion from the study. In addition, subjects with allergies to adhesive or those who felt they would have difficulty abstaining from heavy physical activity during the 24-hour recording period were withdrawn from the study. Subjects were not on any cardioactive medication at the time of the recordings. Volunteers from the MAC seniors program (those over the age of 55 years) had all been subject to a symptom limited ECG stress test prior to entrance into the program to rule out the presence of silent heart disease.

6.3 Testing Protocol

All subjects were tested in the Clinical Neurocardiology lab at the McMaster University Medical Center (MUMC). On arrival at the lab subjects were provided with study details and consent form (Appendix A). Informed consent was obtained from all participants prior to the commencement of any testing procedures. This investigation was approved by the research ethics committee at the MUMC.

6.4 Acute Recordings

All acute ECG signal recordings were performed between 8:30 a.m. and 10:30 a.m. to minimize the influence of the circadian rhythms that exist in heart rate and HRV

indices [37]. Electrode sites were shaved if necessary and thoroughly cleaned with isopropyl alcohol to remove dirt and natural oils from the skin. The ECG signal was recorded through Medi Trace 130 Ag/AgCl stress electrodes in a bipolar lead II setup with the reference electrode positioned just inferior to the mid-line of the left clavicle. As a robust R-wave greatly facilitates identification of the QRS complex, care was taken to avoid DC interference (all nonessential electronic equipment was shut down) and gain settings were adjusted to obtain as clear a signal as possible. The contribution of respiratory sinus arrhythmia to high frequency heart rate variability [38] requires that breathing frequency be monitored along with ECG in studies utilizing power spectral analysis. Respiration was monitored through the same electrode placement by the method of impedance plethysmography. In this technique a 1kHz signal is passed through the subjects thoracic cavity and the impedance between two reference electrodes is monitored. Impedance is inversely proportional to the distance between two points. As such, the expansion of the chest cavity on inspiration would result in a decrease in impedance between two electrodes in the thoracic wall. The resultant respiratory related fluctuations in impedance were sampled at 500Hz and displayed concurrently with the ECG signal.

ECG and respiration were initially recorded for 20 minutes in the supine position. The room was maintained in semi-darkness for the duration of the recording and blankets were provided to ensure a comfortable temperature for the participants. Subjects were encouraged to relax with their eyes closed but to attempt to remain awake for the entire 20 minutes. No effort was made to control the rate or depth of breathing at any time

during this recording. Respiratory frequency was to verify the vagal peak but not used subsequently in this research [9].

Both ECG and respiratory signals were fed through analog recorders and amplified with an HP7807C amplifier. These signals were then digitized using a 1kHz (500 Hz/channel), 12 bit analog-to-digital converter. The resultant waveforms from both channels were displayed simultaneously on a 486/66 MHz personal computer and recorded at 500 samples/sec using a commercially available data acquisition and processing software package (CODAS, DATAQ Instruments Inc. Akron, Ohio, USA). Data files were stored temporarily on the personal computer's hard drive. Following data analysis all file were transferred to long-term storage to digital mini-cassette (Verbatim Datalife) using Colorado backup software. File sizes for the supine data were 2400 Kb.

6.5 Twenty Four-Hour Recordings

Following the supine testing period subjects were requested to wear an ambulatory ECG "Holter" monitor (Model Oxford Medilog 4500 by Oxford Medical Ltd. Oxon, UK) for a period of 24 hours duration. Electrode application sites were shaved if needed and cleaned as per the acute recording procedure. The ECG signal was recorded via a two lead pre-cordial setup (V_1 and V_5) with the two reference electrodes placed just inferior to the mid-line of the right and left clavicles. The ground electrode was positioned on the right side of the lower abdomen in the supra-iliac region. A brief signal test of approximately 20 seconds in duration was performed automatically prior to the initiation of the recording to ensure that a waveform of sufficient quality for analysis could be obtained on both channels. In the case of a poor quality signal on one or both

channels, the corresponding electrodes were repositioned and/or the existing sites were more thoroughly cleaned and prepared. Following a positive signal test the monitor performed a short calibration and the recording was subsequently initiated. The ECG electrodes were further secured to the chest with 3M Transpore™ hypoallergenic surgical tape to minimize movement artifact and to reduce the chance of the wires becoming disconnected during the recording. ECG waveforms from both channels were simultaneously recorded at a rate of 125 samples/second and stored on a standard, normal bias 60-minute audiotape for a period of 24 hours. Upon completion of the recording subjects were instructed to remove and dispose of the electrodes, switch the monitor off and return it to the lab or MAC seniors program (for the elderly subjects) at a convenient time arranged during the initial phone interview).

To aid in the analysis of the Holter tapes subjects were required to complete an activity diary concurrently with the 24-hour recording. Start and finish times for sleep, meals, visits to the bathroom and other activities were listed. Participants were encouraged to maintain their daily schedules but instructed to abstain from heavy physical activity or showering while wearing the monitor.

6.6 Signal Processing & Data Analysis

Data files from the acute recordings were visually inspected and the two signals (ECG and respiration) were separated through an advanced post-acquisition processing software. A detection algorithm was utilized to label the individual QRS complexes and compute R-R intervals from the raw ECG signal. An R-R tachogram was then constructed using the interval data.

The compensatory pause following an ectopic beat may be erroneously attributed to high frequency, vagally modulated heart rate variability and thus confound the results of power spectral analysis [39, 40]. As such, the R-R interval tachograms were visually inspected for the presence of ectopic beats prior to the application of autoregressive modeling procedures. In cases in which the data set was corrupted by an inordinate number of ectopics (>3 per 5 min), additional post-acquisition processing was performed to select and remove an uncontaminated segment of data. Files from which appreciable segments (>512 data points/~4-5 minutes) of untainted data could not be extracted were excluded from the analysis. Small numbers of ectopics present in the accepted data segments were corrected for using an interpolation algorithm. Detection of ectopic beats by the algorithm was accomplished by setting a threshold value by which a beat may differ from the one immediately preceding it (e.g. 0.90-1.10xprevious R-R interval). Beats exceeding this value were labeled as ectopic and subsequently corrected. The amount of 'normal' variability inherent in the heart rate of a young subject can differ substantially from that of an elderly individual Figure 6.1. Therefore, the filter was individually adjusted to accommodate these age-related differences following the visual inspection of the data.

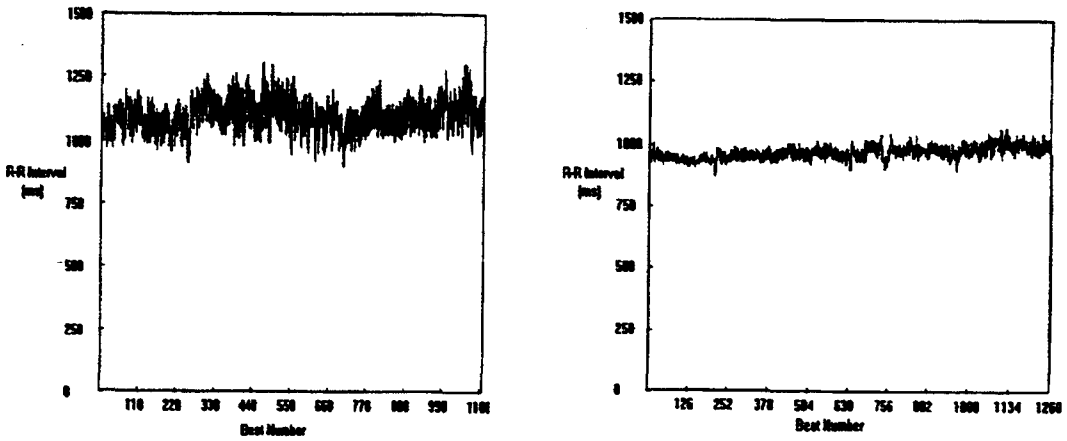

Figure 6.1: The R-R interval tachograms of (*left*) young subject, and (*right*) older subject [9].

6.6.1 Computation of power-law scaling

Power-Law scaling is applied to the acutely recorded HRV signal recorded from healthy subjects for 20 minutes in the supine position. The acute data provided 1024 RR intervals and permitted a computation of the power spectra. The RR interval signal is then converted into a heart rate (HR) signal for analysis. Linear interpolation at a rate of 1Hz is then applied to the HR signal to obtain adequate number of samples to perform a Fourier transform. Furthermore, Fourier transform and power spectral density analysis are applied to the HR signal for power-law scaling to be achieved.

6.6.2 Computation of approximate entropy

ApEn was computed using methods described in section 5.3. We used 1024 RR intervals obtained from the acute HRV signal recorded from healthy subjects. ApEn is obtained for m=2, and r=0.15 of standard deviation.

6.6.3 Computation of detrended fluctuation analysis

According to C. K. Peng et al. [28], DFA measure was applied to long signal length of 16384 and short sets of 4096 beats. They reported that a long data set results in improvement for the distinction between groups, hence the use of data sets of length 8192 seemed to be a statistically reasonable choice.

In this study, DFA measures are applied to two different signal lengths to explore the effect of data length on the measurement. The first data length is 1024 beats from the acute recording. The box size for this data length ranged from 4 to ~ 861 beats. The second data length is 8192 beats from the twenty four-hour recording (approximately 2-2.5 hours). The box size for this data length ranged from 4 to ~ 6889 beats. For both data lengths, box sizes larger than the ones stated would give a less accurate fluctuation value because of the finite-length of the signal.

6.6.4 Computation of surrogate data and correlation dimension

Surrogate data analysis technique is applied to the acute data, allowing an analysis to be applied to 1024 points of RR interval. The RR interval signal is then converted into a heart rate (HR) signal for analysis. Fourier transform is then applied to the HRV signal length with a sampling frequency of 1Hz. Next, the phase of the data set is randomized and its power spectra is computed. This process is repeated 10 times, using different random seeds to acquire 10 different phase randomized surrogate data sets.

Furthermore, correlation dimension is computed from the original HRV signal, as well as from its corresponding phase randomized surrogate data sets. The correlation

dimension is calculated for tolerances ranging from r_{min} to r_{max} for each embedded dimension. The embedded dimensions vary from $m = 2$ to 20 for each data set.

6.7 Testing of Nonlinear Dynamic Indices

To test different nonlinear indices, we need to generate data sets exhibiting chaotic behaviour. A simple system that produces a chaotic signal is the Logistic Map [1]. Also, we will be testing the nonlinear indices developed in the previous chapter on several models of artificial signals that have different percentages of added noise.

6.7.1 The Logistic map

The logistic map is a recursive simple equation for a parabola:

$$\mathbf{y = k\,x\,(1 - x)} \tag{6.1}$$

where **x** is a variable ($0 \leq \mathbf{x} \leq 1$) and **k** is a parameter ($0 \leq \mathbf{k} \leq 4$). The logistic equation contains both linear and nonlinear components that are better seen when the equation is expressed in another form:

$$\mathbf{y = k\,x - k\,x^2} \tag{6.2}$$

The **kx** term is the linear portion of the equation, while the $\mathbf{kx^2}$ term is the nonlinear portion. If we choose particular values for **k** and **x**, we can substitute them into the equation and get a value for **y**. If we now substitute **y** as the new value for **x**, we obtain a new value for **y** (**k** remains the same). When we run this recursion several hundreds of iterations, a graph representing the dynamic behaviour of the system can be obtained [1].

For the initial condition $\mathbf{x} = 0.05$, $\mathbf{k} = 2.8$, and iterate the equation 100 times, we see that after a short oscillation, the system settles into a predictable and stable output (a flat line, Figure 6.3(a)). The system is stable because the linear portion of the equation is

dominant. By increasing **k** to 3.3 and keeping the initial value of **x** the same, a sudden qualitative change in behaviour of the system occurs – it begins to oscillate between two different states as the nonlinear portion of the equation becomes manifest (Figure 6.3(b)). Increasing **k** further to 3.8, the system suddenly begins to exhibit strikingly aperiodic, seemingly random, behaviour – chaos – as the nonlinear term becomes dominant (Figure 6.3(c)). The entire range of behaviour is summarized in the bifurcation diagram illustrated in Figure 6.2.

Three models of the logistic map are introduced for testing to differentiate between regularity and irregularity (chaos). Model A, **k**=3.3 (regular, predictable) Figure 6.3(b). Model B, **k**=3.6 (less regular, and less predictable). Model C, **k**=3.8 (irregular, chaotic) Figure 6.3(c).

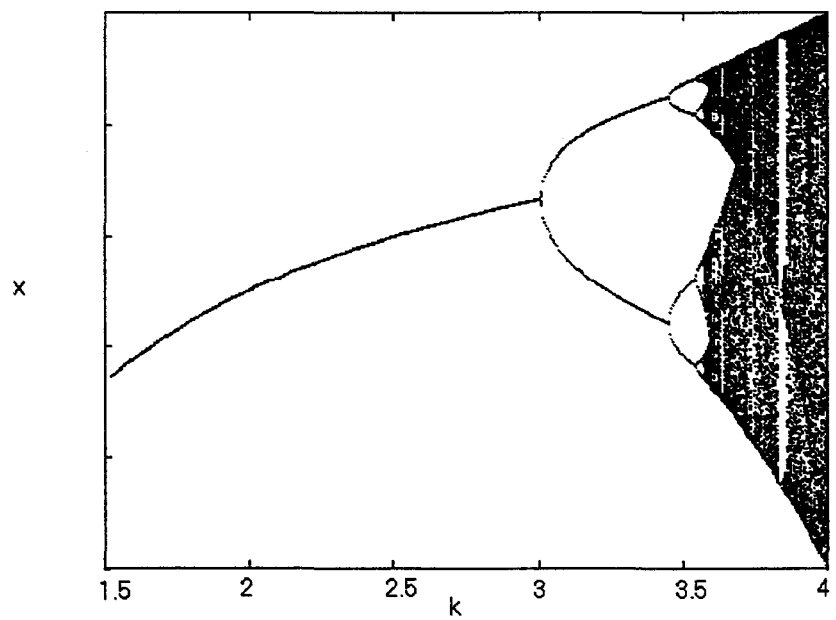

Figure 6.2: The bifurcation diagram of the logistic map.

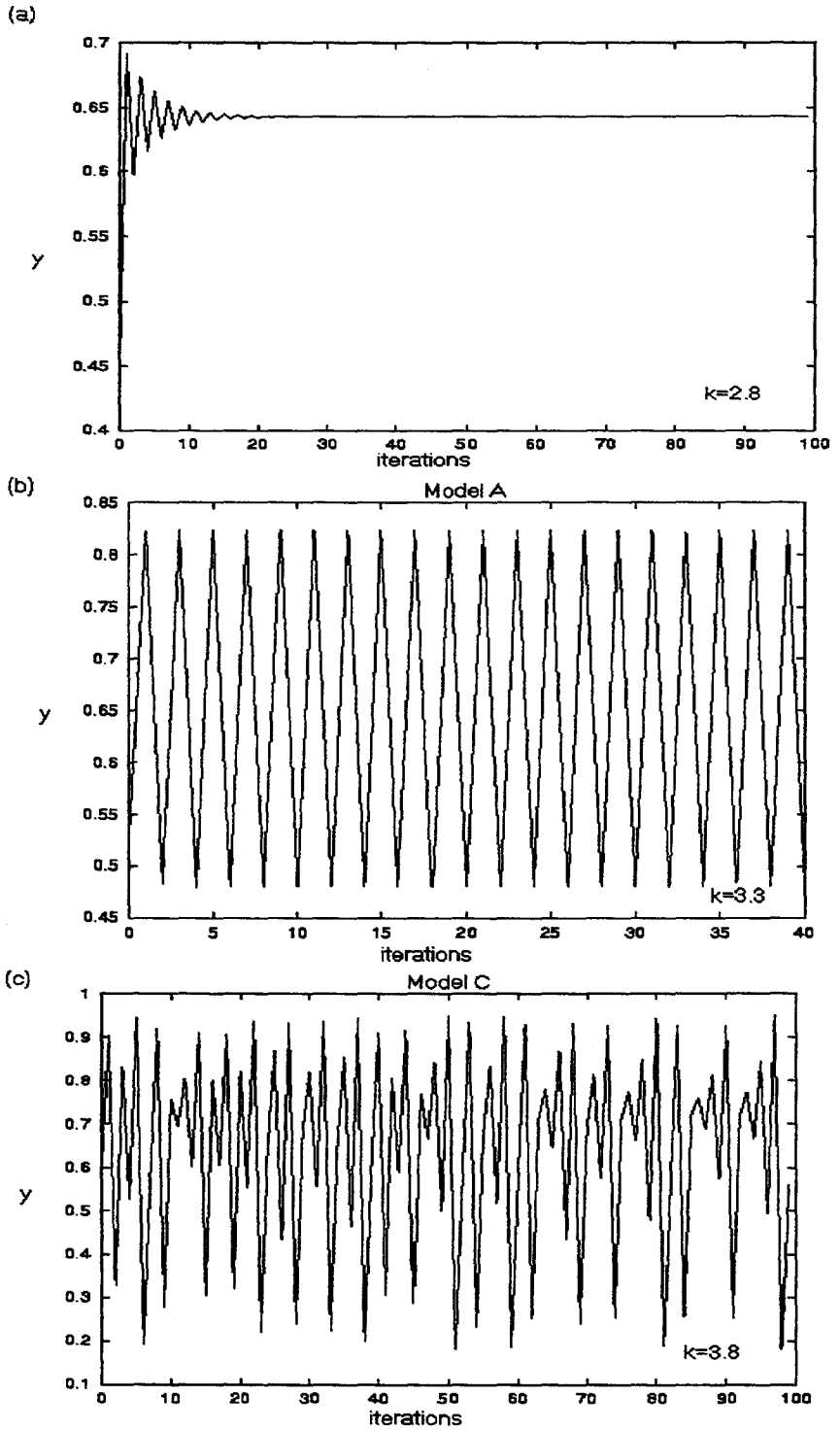

Figure 6.3: The logistic map, (a) k=2.8, stable state, (b) k=3.3, oscillation between two states, (c) k=3.8, chaotic signal.

6.7.2 Signal with added noise

Similarly, the following five signal models are introduced to test the nonlinear indices:

- Model D, consists of a sine wave of amplitude 1 at a frequency of 0.1Hz and which was sampled at 68.33Hz. A 20% white noise was added. This signal is relatively regular and predictable.
- Model E, consists of the same sine wave with 50% added white noise (less regular, and less predictable).
- Model F, consists of the same sine wave with 90% added white noise (irregular).
- Model G, consists of white noise (random).
- Model H, consists of Brownian noise (correlated).

These signal models are shown in Figure 6.4.

We anticipate that as the signal gets corrupted with increasing amounts of noise, the nonlinear indices will tend towards that of random signal.

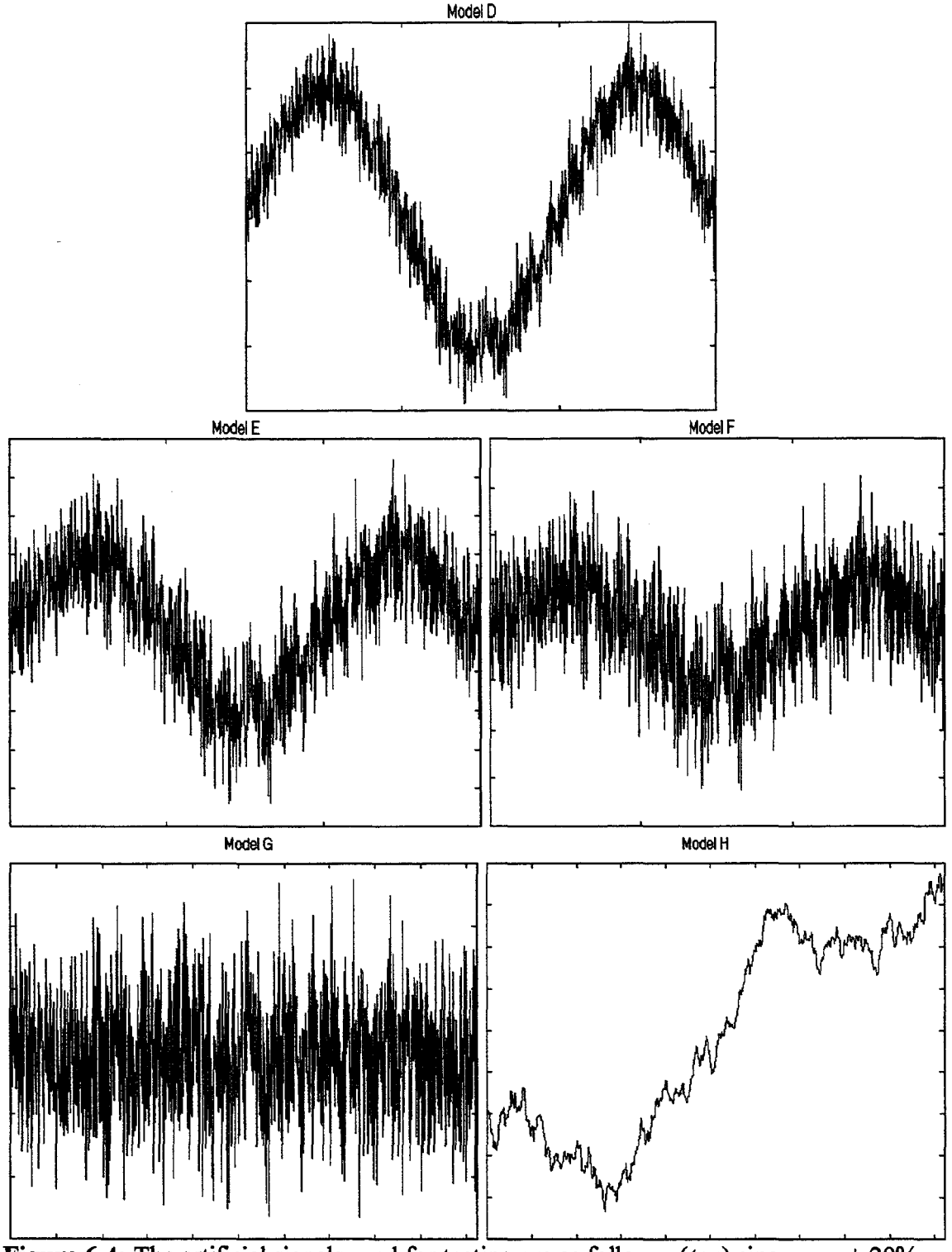

Figure 6.4: The artificial signals used for testing are as follows: (*top*) sine wave + 20% white noise. (*middle left*) sine wave + 50% white noise. (*middle right*) sine wave + 90% white noise. (*bottom left*) pure white noise. (*bottom right*) Brownian noise.

6.7.3 Testing of power-law scaling

Tests were conducted to verify power-law scaling using white noise and Brownian noise. We find that for white noise, $\beta = 0$ (Model G), since the frequency is spread across the spectrum. As for Brownian noise, $\beta \approx -3$ (Model H), as shown in Figure 6.5.

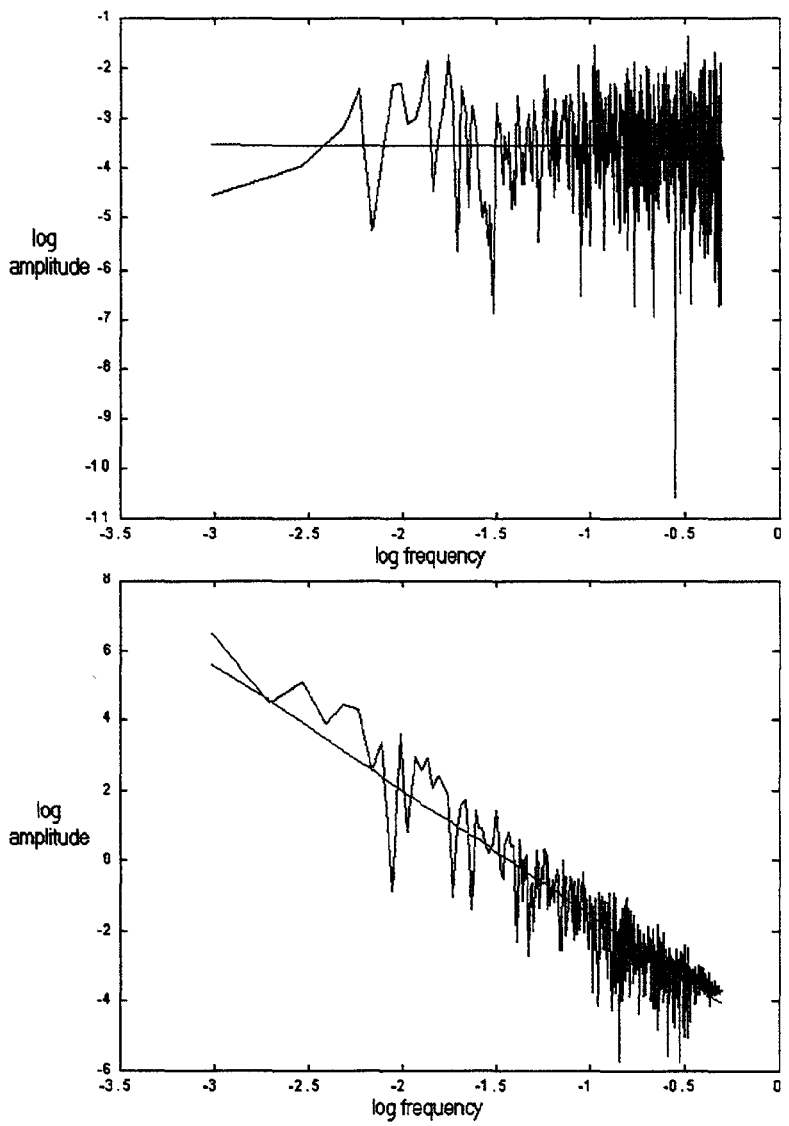

Figure 6.5: Testing power-law scaling on white noise (*top*), and on Brownian noise (*bottom*).

6.7.4 Testing of approximate entropy

Approximate entropy is tested on the data generated through the logistic map (Figure 6.3) and then on the artificial signals (Figure 6.4). These results are stated in table 6.1. We find that the results are consistent with our hypothesis, as the ApEn measure decreases with regularity.

Signals for Testing	ApEn
Logistic map → k = 3.3 (Model A)	0.0
Logistic map → k = 3.6 (Model B)	0.218
Logistic map → k = 3.8 (Model C)	0.449
Artificial signal → sine + 20% noise (Model D)	1.304
Artificial signal → sine + 50% noise (Model E)	1.531
Artificial signal → sine + 90% noise (Model F)	1.543

Table 6.1: Results acquired from testing the approximate entropy.

6.7.5 Testing of detrended fluctuation analysis (DFA)

Testing of the DFA algorithm is similar to that of testing the power-law scaling algorithm. Our results indicate that the scaling exponents α was 0.5 for white noise and was 1.5 for Brownian noise (Figure 6.6). These results agree with the predicted value, since Brownian noise has high correlation, while white noise has none. Therefore, we can conclude that α decreases with irregularity.

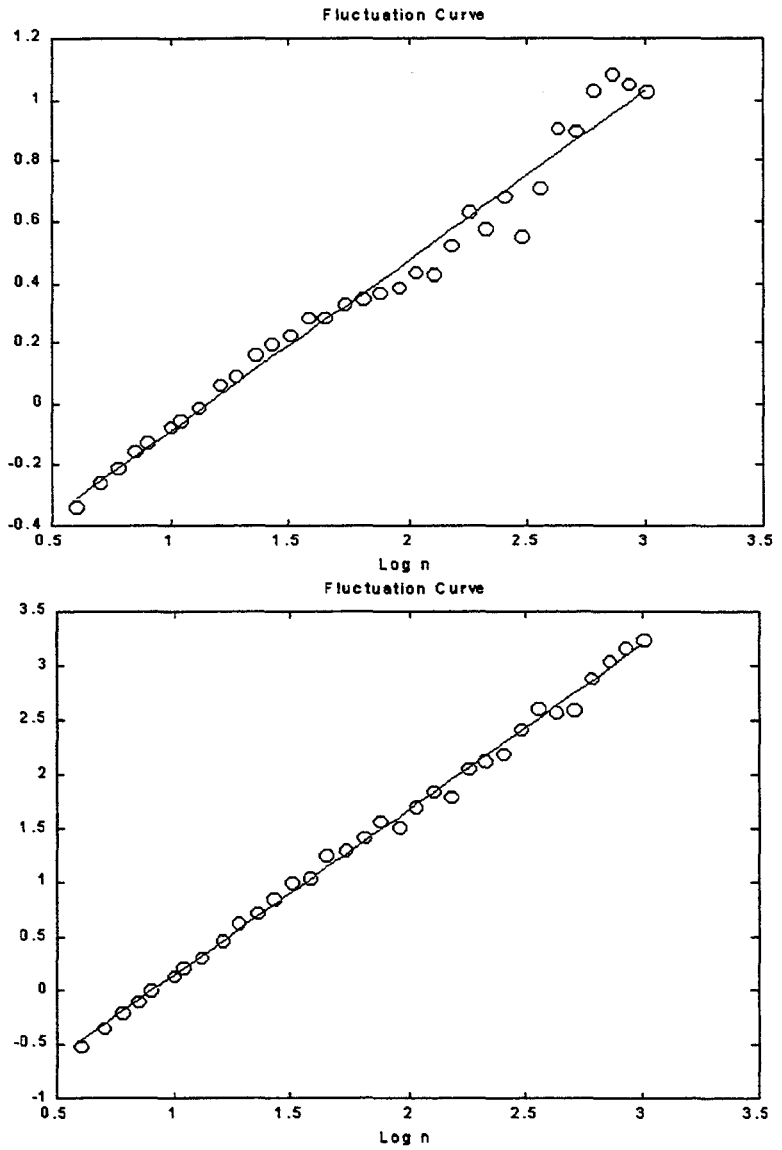

Figure 6.6: Testing the DFA scaling exponent on white noise (*top*), and on Brownian noise (*bottom*).

6.7.6 Testing of surrogate data procedure

The surrogate data technique was applied to three sets of artificial data:

- The first data set consists of a summation of three sine waves. The signal is sampled at 1Hz. The first sine wave was at 0.1Hz, the second sine wave was at 0.2Hz and the third sine wave was at 0.4Hz.

- The second data set similarly consists of a summation of five sine waves. These were at frequencies of 0.1, 0.2, 0.3, 0.4, and 0.45Hz.
- The third data set consisted of white noise (Model G).

The results shown in Figure 6.7 show that randomizing the phase will not affect the Fourier transform of the data set. Figure 6.7 shows that the FFT of the original data and the surrogate data (after phase randomization) are identical.

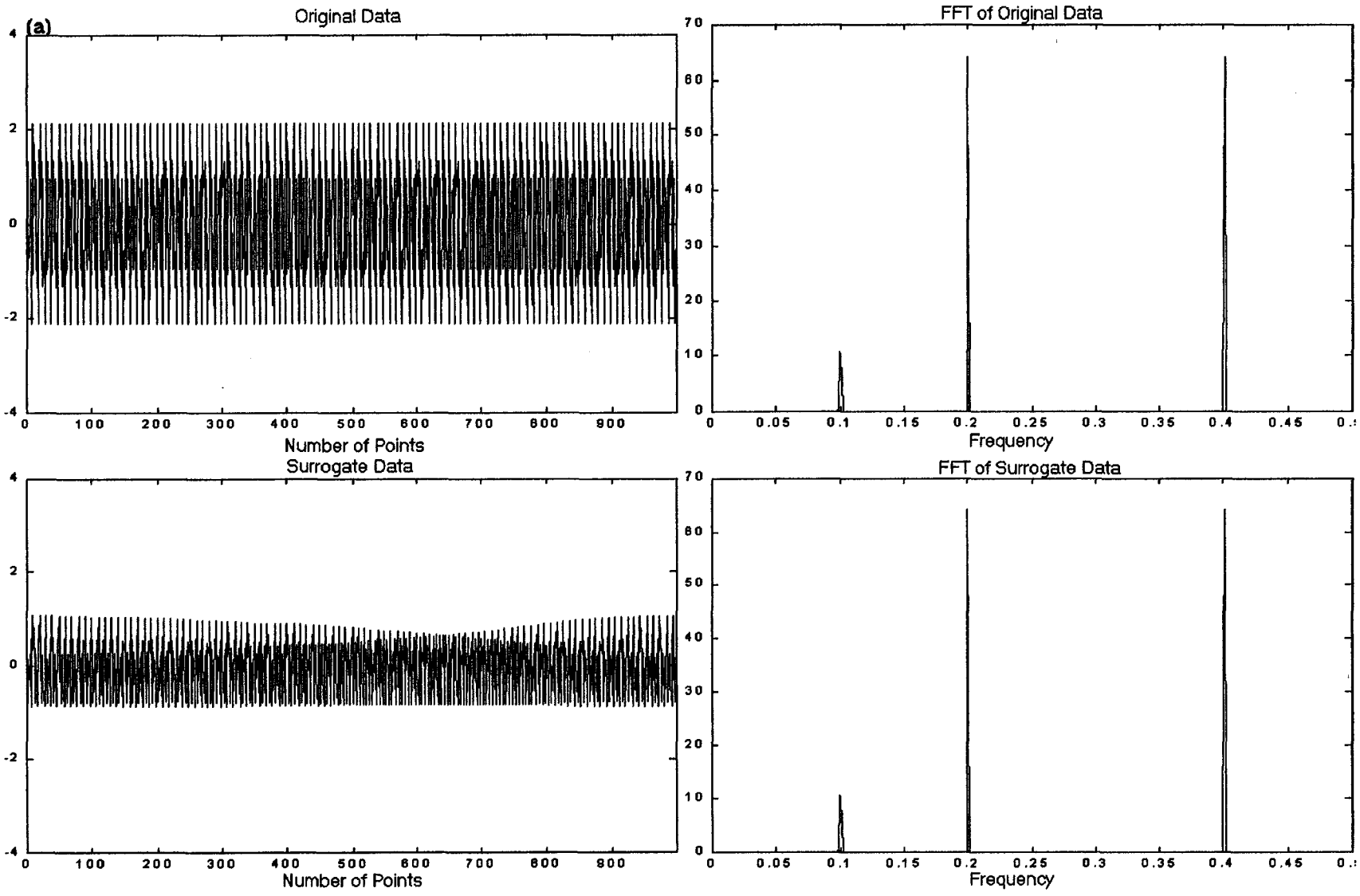
(a)
Original Data
Number of Points
FFT of Original Data
Frequency
Surrogate Data
Number of Points
FFT of Surrogate Data
Frequency

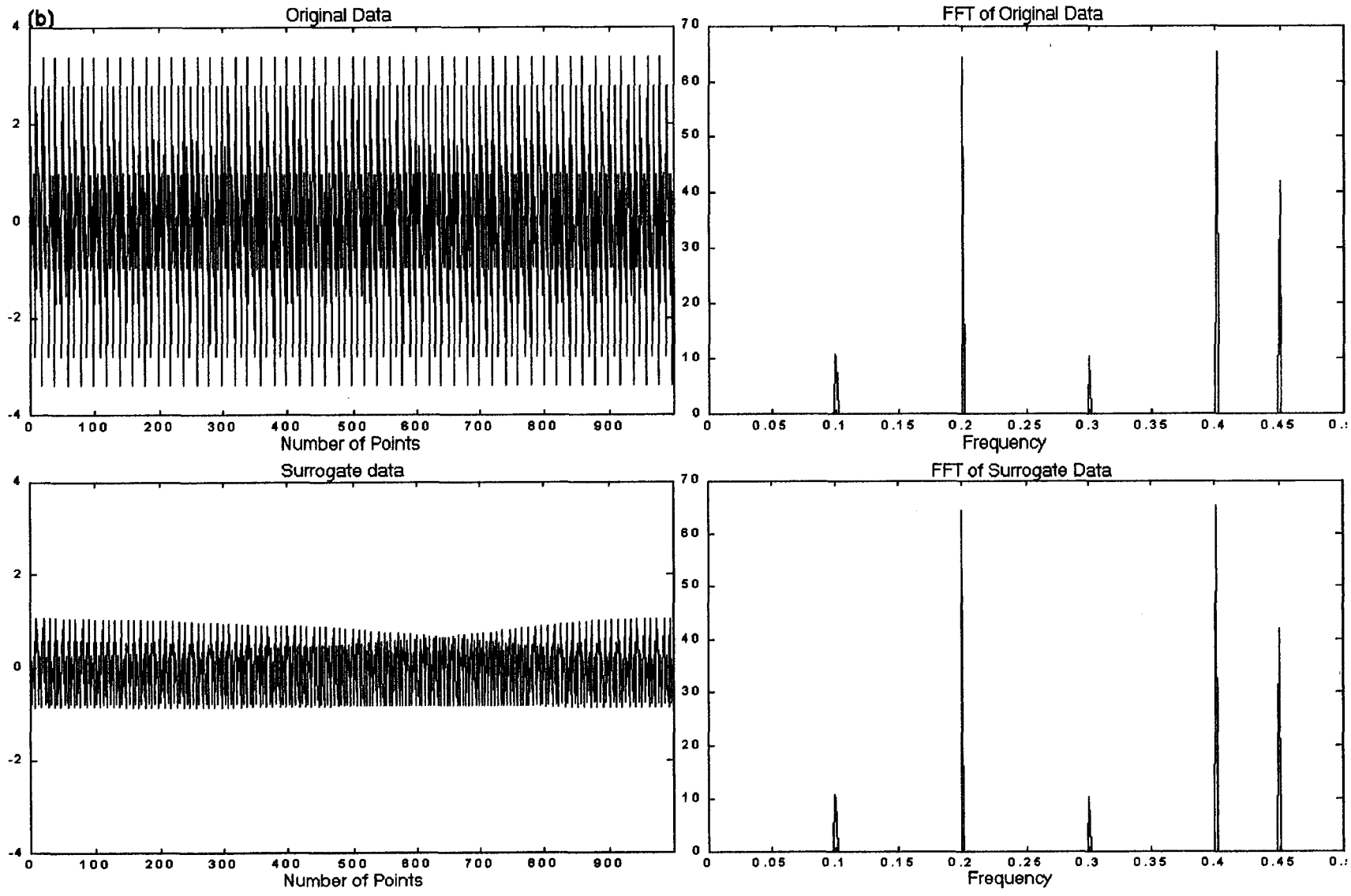
(b)
Original Data
Number of Points
FFT of Original Data
Frequency
Surrogate data
Number of Points
FFT of Surrogate Data
Frequency

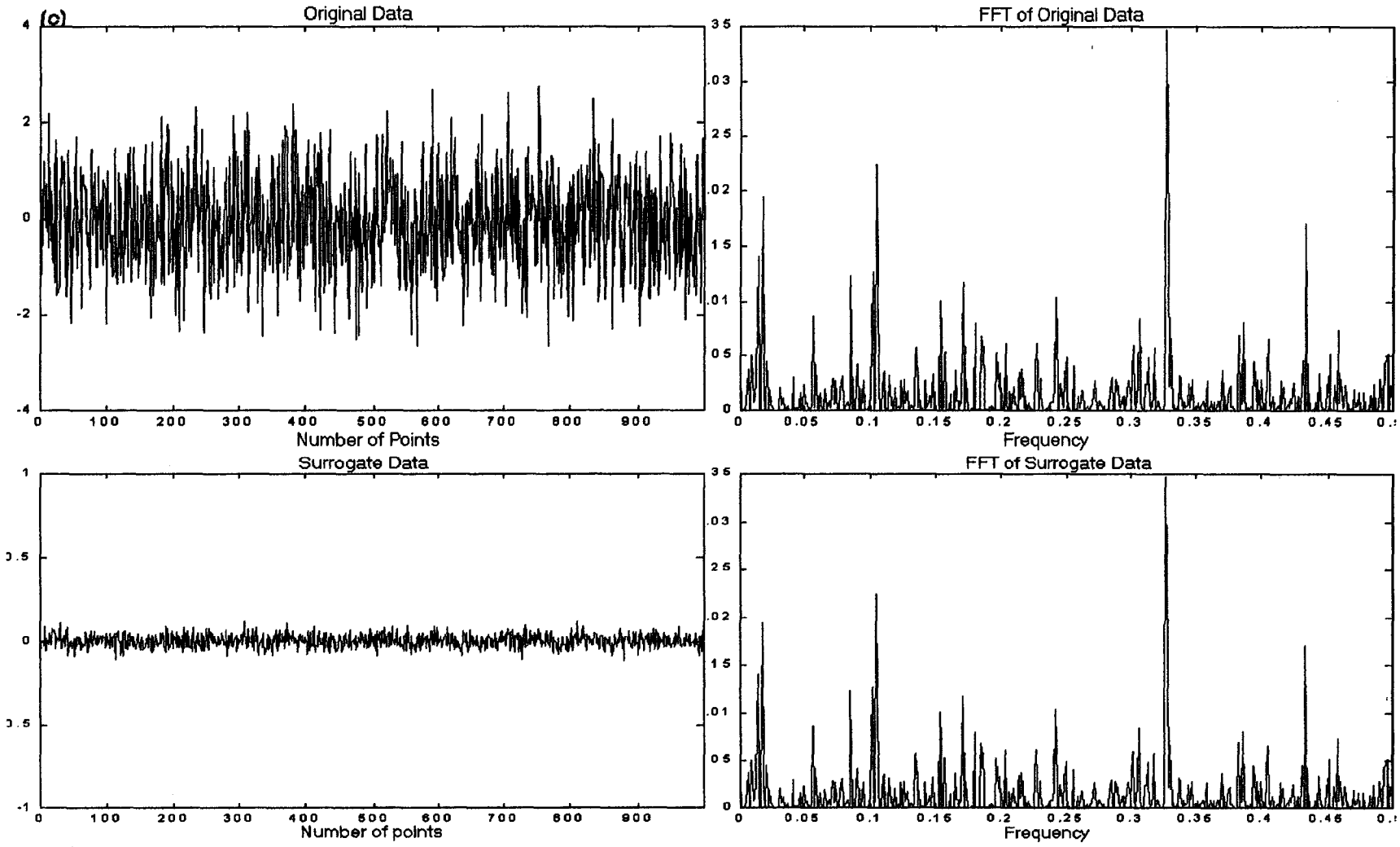

Figure 6.7: The numerical data of mixed sine waves of (a) three (b) five frequency waveforms respectively, and of (c) white noise; also shown are the original data and surrogate data sets with their corresponding power spectra.

6.8 Statistics

The nature of existing relationships between age and HRV parameters were examined with multiple regression analyses. The strength of these associations was characterized by R measures. Differences between age groups were tested using analysis of variance (ANOVA). Significance tests were performed with $p \leq 0.05$ level.

6.9 Conclusion

In this chapter, we discussed the acquisition and processing of the signal used in this study. We also tested all the nonlinear indices used to test our hypothesis. Our findings suggest a consistency in our hypothesis.

Chapter 7

Effects of Aging on the Nonlinear Dynamics of the HRV Signal

7.1 Introduction:

In this chapter, we will examine the results of nonlinear analysis of the HRV signal to understand the effects of aging in the human cardiovascular regulatory system.

7.2 Effect of Aging on Power-Law scaling of the HRV signal

The scatter plot of power-law scaling in relation to age is shown in Figure 7.1. There is a linear reduction in the slope β with age. The value of the F statistic (ANOVA) is 6.649 ($p < 0.001$), and R is 0.475 ($p < 0.001$). Table 7.1 shows the mean value of the power-law scaling $\beta \pm$ standard deviation for each age group.

7.3 Effect of Aging on Approximate Entropy of the HRV signal

The scatter plot of approximate entropy in relation to age is shown in Figure 7.2. We can observe a consistent decrease in the value of ApEn with age. The value of the F statistic (ANOVA) is 7.82 ($p < 0.001$), and R is 0.519 ($p < 0.001$). Table 7.2 shows the mean value of the approximate entropy ApEn $\pm$ standard deviation for each age group.

Age Groups	β
5-12 years	-1.162 ± 0.388
13-17 years	-1.483 ± 0.399
18-30 years	-1.52 ± 0.58
31-60 years	-1.78 ± 0.34
61-78 years	-1.95 ± 0.6

Table 7.1: The values of **β** according to each age group. **β** values are expressed as mean ± S.D.

Age Groups	ApEn
5-12 years	1.4557 ± 0.093
13-17 years	1.4275 ± 0.081
18-30 years	1.395 ± 0.105
31-60 years	1.349 ± 0.107
61-78 years	1.272 ± 0.135

Table 7.2: The values of ApEn according to each age group. ApEn values are expressed as mean ± S.D.

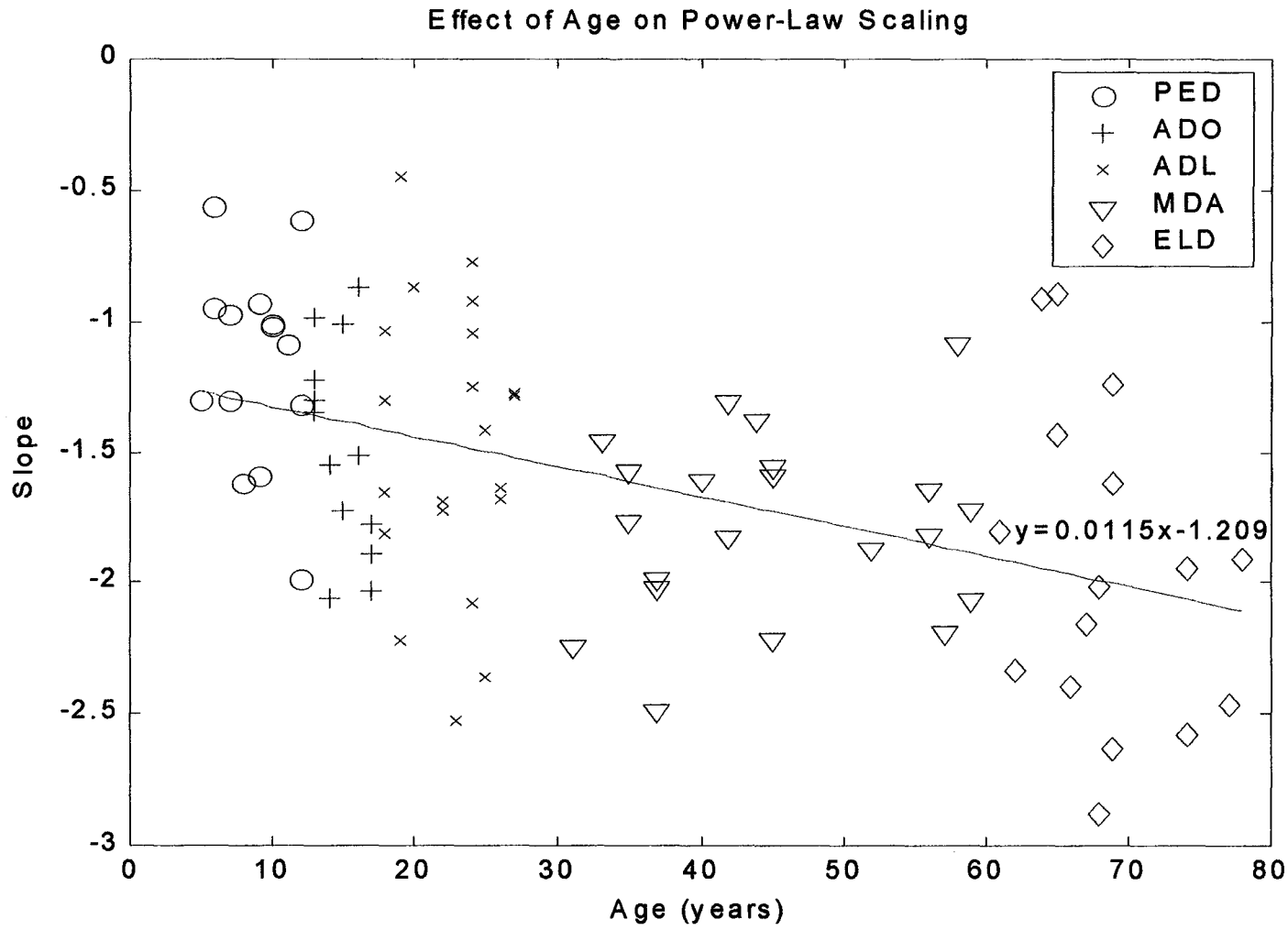

Figure 7.1: Effect of age on power-law scaling. Scatter plot shows the slope **β** vs. age.

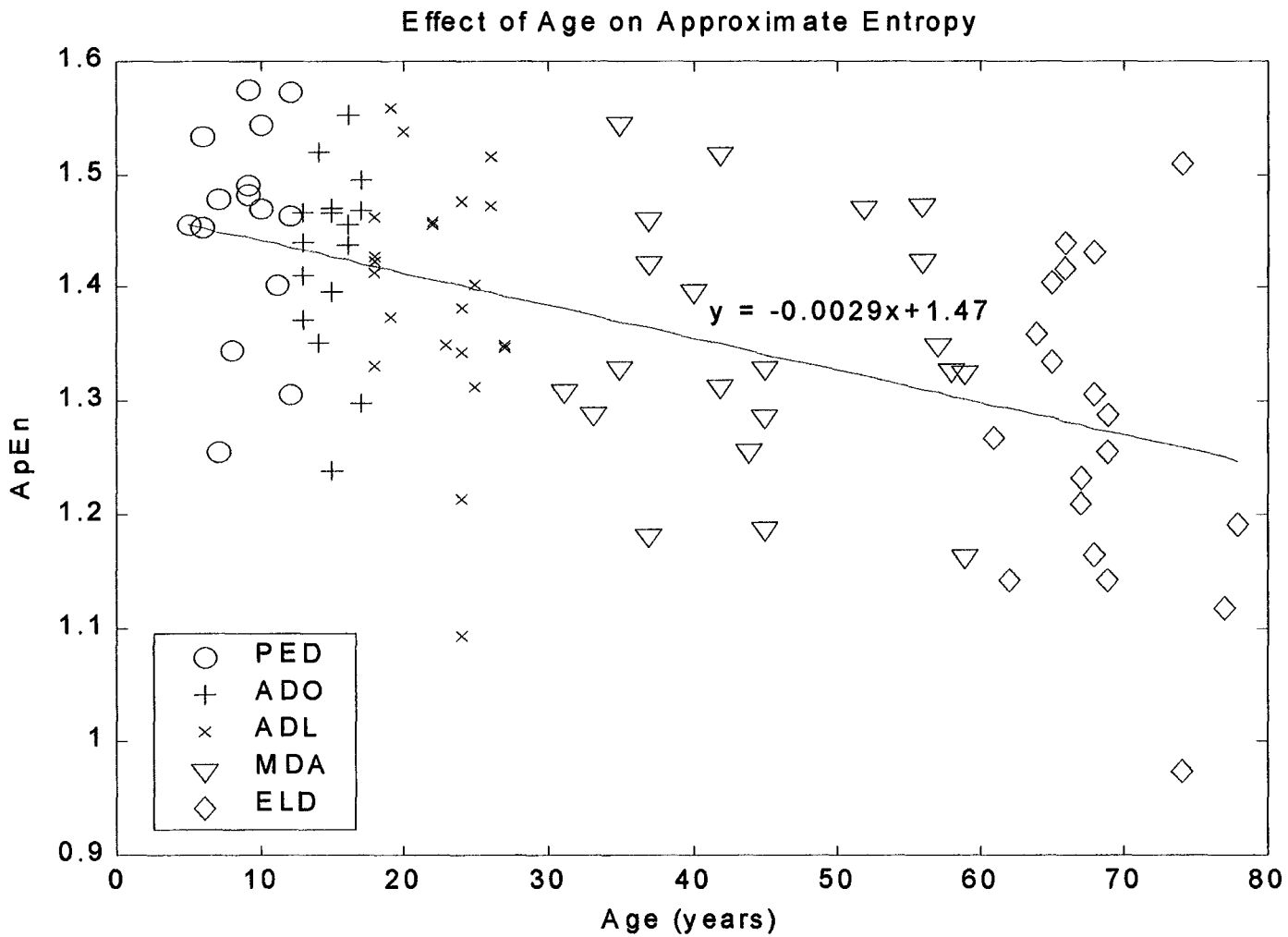

Figure 7.2: Effect of age on approximate entropy. Scatter plot shows the ApEn value vs. age.

7.4 Effect of Aging on Detrended Fluctuation Analysis of the HRV signal

Two types of detrended fluctuation analysis are applied to the HRV signal in this study. The short-term DFA, using only 1024 points acquired from acute recordings and the long-term DFA, using 8192 points acquired from twenty four-hour recordings were computed. The results of this technique on both short-term and long-term are as follows:

7.4.1 Short-Term DFA

The scatter plot of the short-term DFA scaling exponent is shown in Figure 7.3. This graph shows the short-range scaling exponent α_1 (<11 beats) vs. the long-range scaling exponent α_2 (> 11 beats). The value of the F statistic used for the ANOVA of the short-range DFA scaling exponent α_1 is 7.535 ($p < 0.001$). As for the ANOVA of the long-range DFA scaling exponent, α_2 is 4.841 ($p < 0.001$). This shows statistical significance for both α_1 and α_2. In Figure 7.3, we can observe the concentration of younger subjects at smaller α_1 and α_2 while the older subjects are concentrated at larger α_1 and α_2. Table 7.3 shows the mean values of α_1 and α_2 and their corresponding standard deviation for each age group.

7.4.2 Long-Term DFA

The scatter plot of the long-term DFA scaling exponent is shown in Figure 7.4. This graph shows the short-range scaling exponent α_1 (<11 beats) vs. the long-range scaling exponent α_2 (> 11 beats). The value of the F statistic used for ANOVA of the short-range DFA scaling exponent α_1 is 1.922. As for ANOVA of the long-range DFA

scaling exponent, α_2 is 4.06 ($p < 0.01$). The latter value, α_2, shows statistical significance. However, α_1 is not statistically significant between age groups for long-term DFA calculations. These results are also shown in Figure 7.4, where we can observe that both young and old subjects are spread all over the α_1 spectrum. However, there is a higher concentration of older subjects at large α_2 values, as well as a higher concentration of younger subjects at smaller values of α_2. Table 7.4 shows the mean value of α_1 and α_2 and their corresponding standard deviation for each age group.

Age Groups	α_1	α_2
5-12 years	0.774 ± 0.204	0.667 ± 0.082
13-17 years	0.825 ± 0.191	0.809 ± 0.162
18-30 years	0.923 ± 0.233	0.833 ± 0.107
31-60 years	1.079 ± 0.252	0.847 ± 0.127
61-78 years	1.138 ± 0.289	0.86 ± 0.172

Table 7.3: The values of the short-term scaling exponents α_1 and α_2 according to each age group. α_1 and α_2 values are expressed as mean ± S.D.

Age Groups	α_1	α_2
5-12 years	1.052 ± 0.218	0.961 ± 0.081
13-17 years	1.153 ± 0.21	0.989 ± 0.087
18-30 years	1.152 ± 0.166	0.958 ± 0.104
31-60 years	1.238 ± 0.187	1.003 ± 0.092
61-78 years	1.204 ± 0.205	1.076 ± 0.102

Table 7.4: The values of the long-term scaling exponents α_1 and α_2 according to each age group. α_1 and α_2 values are expressed as mean ± S.D.

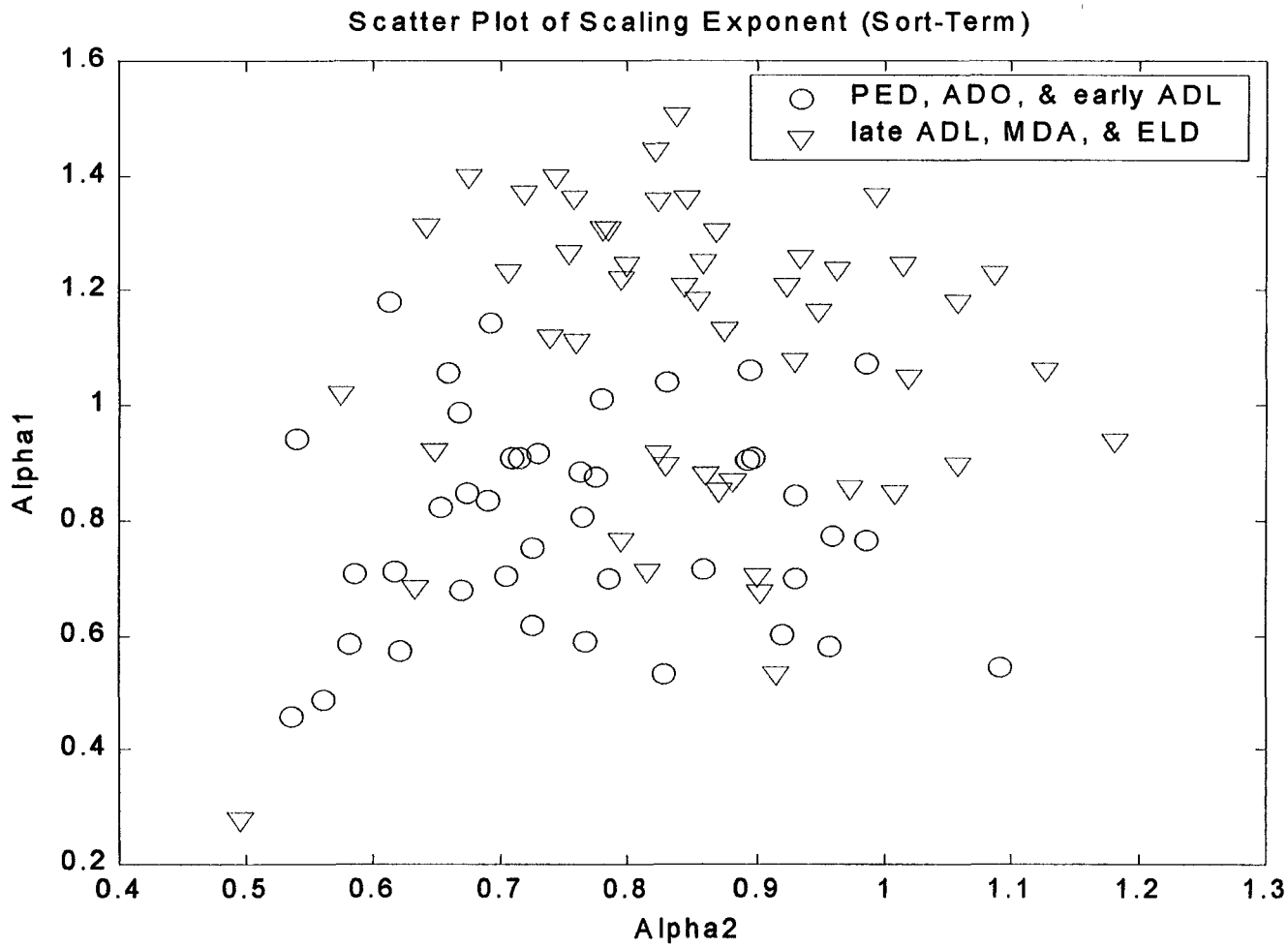

Figure 7.3: Scatter plot of short-term DFA. Scatter plot shows the α_1 value vs. α_2.

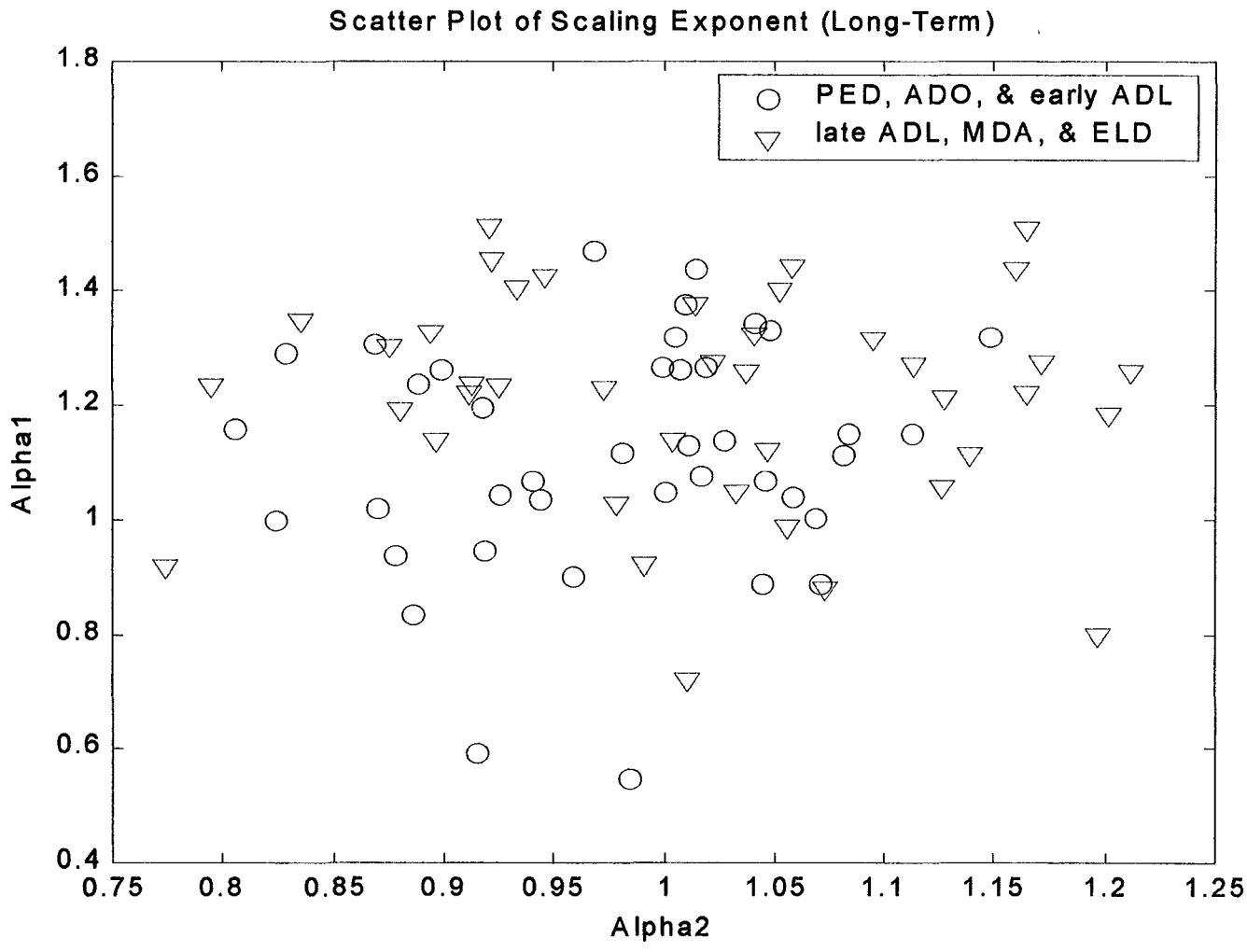

Figure 7.4: Scatter plot of long-term DFA. Scatter plot shows the α_1 value vs. α_2.

7.5 Correlation Dimension of the HRV Signal

The objective of this technique is to test the general hypothesis that surrogate data technique can help identify if the heart rate variability signal is chaotic or not. Hence, correlation dimension is applied to both the original data set and to 10 different realizations of surrogate data sets. The results shown in Figure 7.5 are for two subjects from the pediatric group. The correlation dimension is plotted vs. the embedded dimensions that vary from 2 to 20 for each subject. Similarly, the results in Figure 7.6 to Figure 7.9 show results of such analysis for the adolescent group, the adult group, the middle-aged group, and the elderly group respectively.

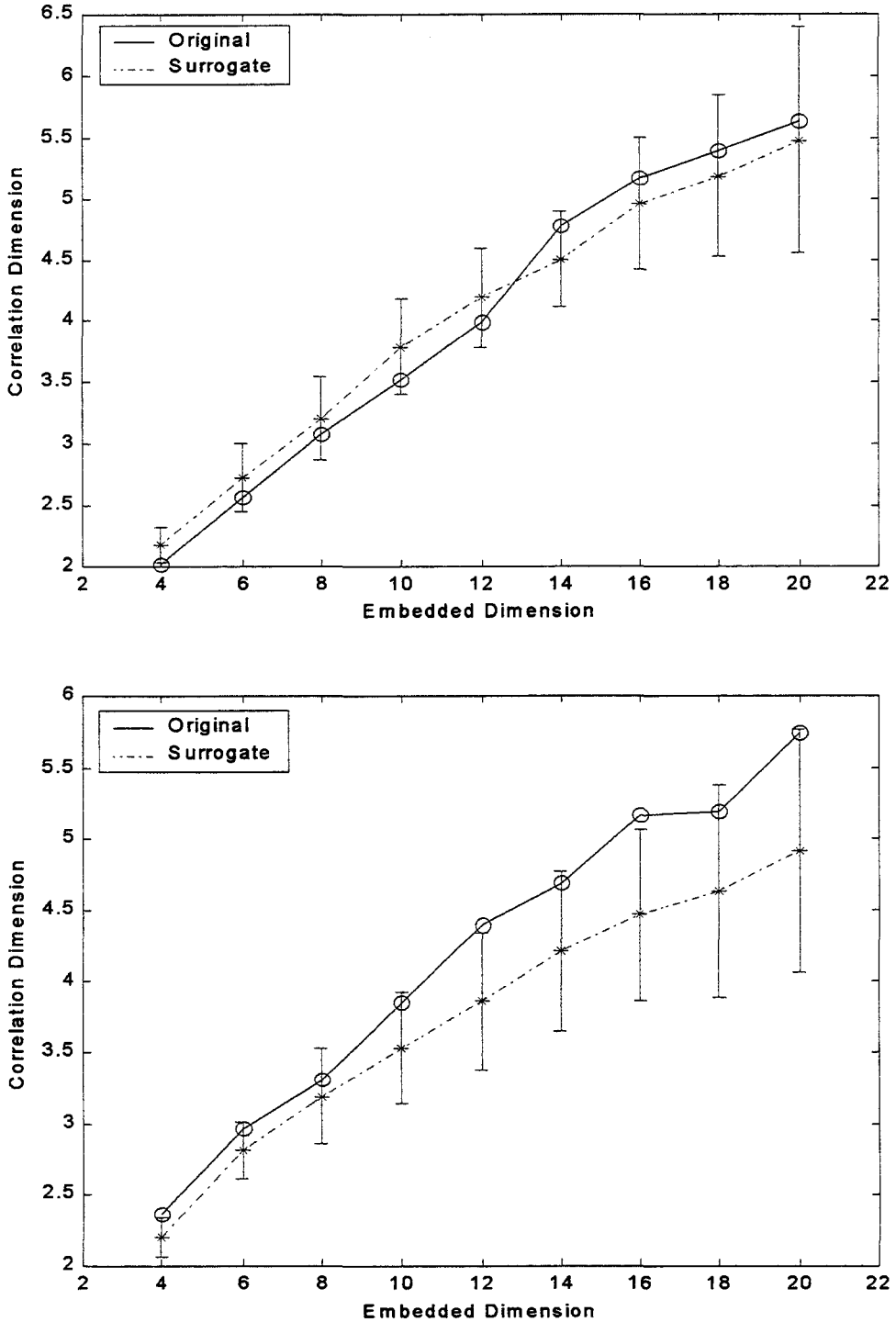

Figure 7.5: Correlation dimension of two subjects from the pediatric group. The correlation dimension of the original data and for its corresponding surrogates (and their standard deviation) is plotted vs. the embedded dimension.

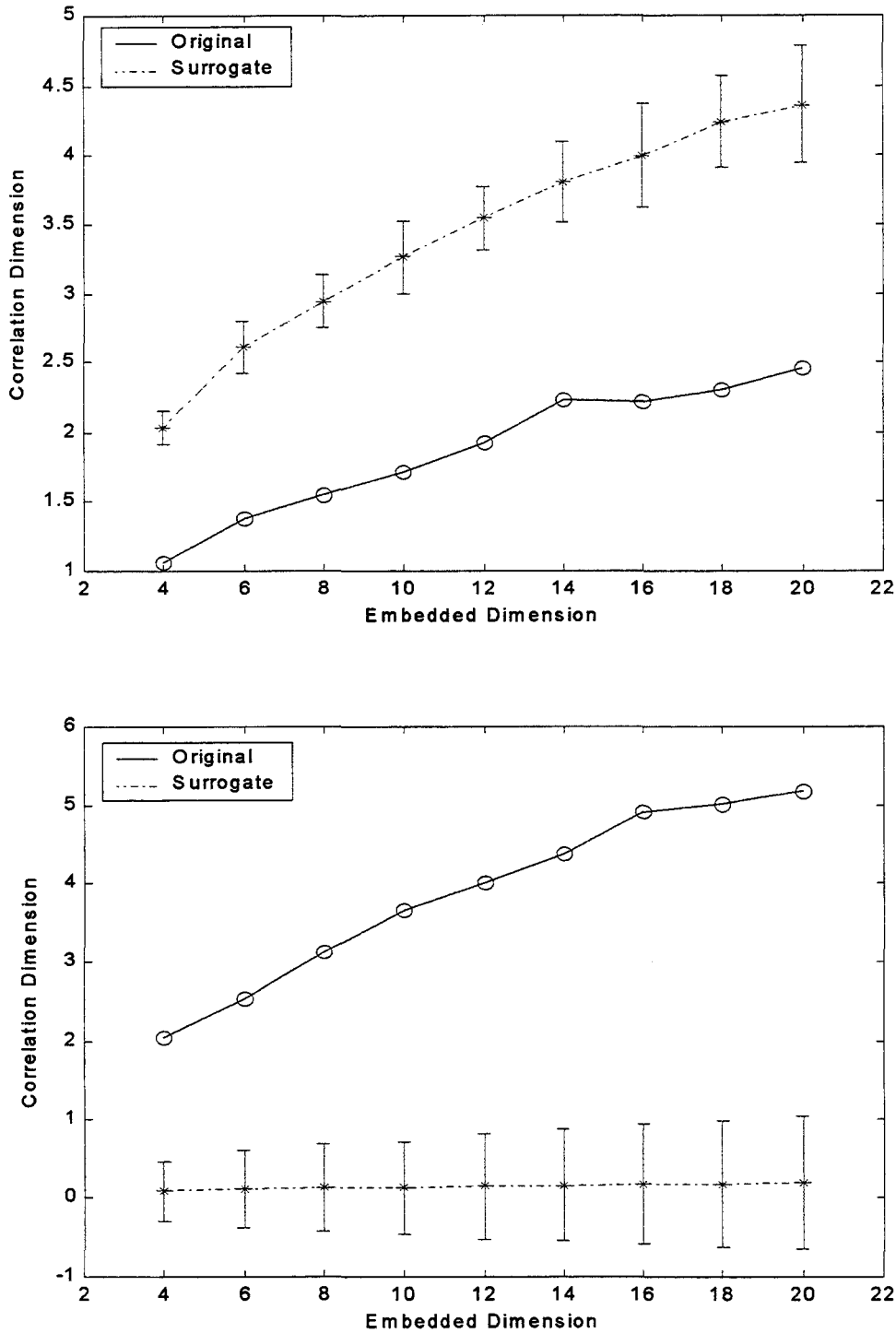

Figure 7.6: Correlation dimension of two subjects from the adolescent group. The correlation dimension of the original data and for its corresponding surrogates (and their standard deviation) is plotted vs. the embedded dimension.

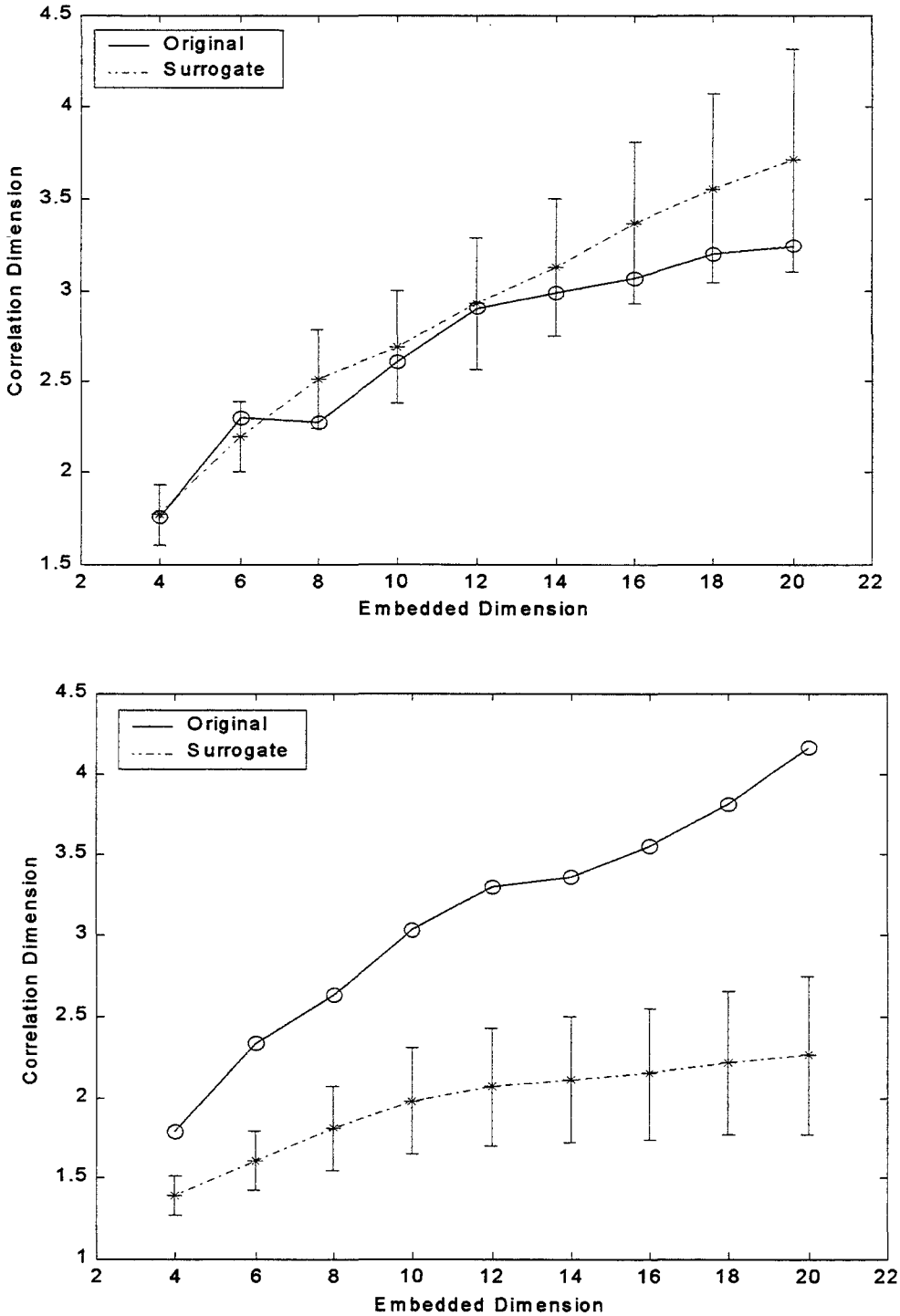

Figure 7.7: Correlation dimension of two subjects from the adult group. The correlation dimension of the original data and for its corresponding surrogates (and their standard deviation) is plotted vs. the embedded dimension.

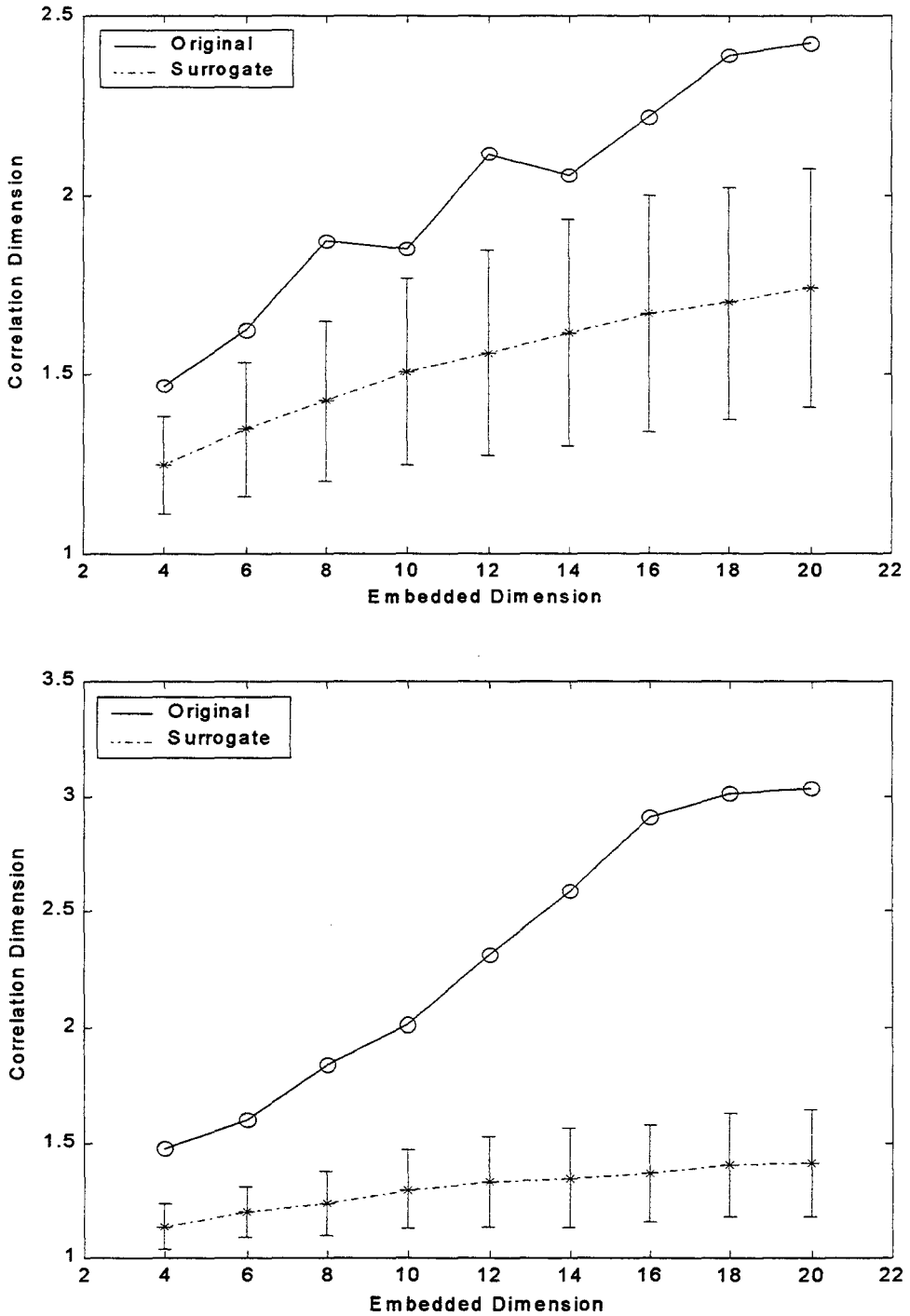

Figure 7.8: Correlation dimension of two subjects from the middle aged group. The correlation dimension of the original data and for its corresponding surrogates (and their standard deviation) is plotted vs. the embedded dimension.

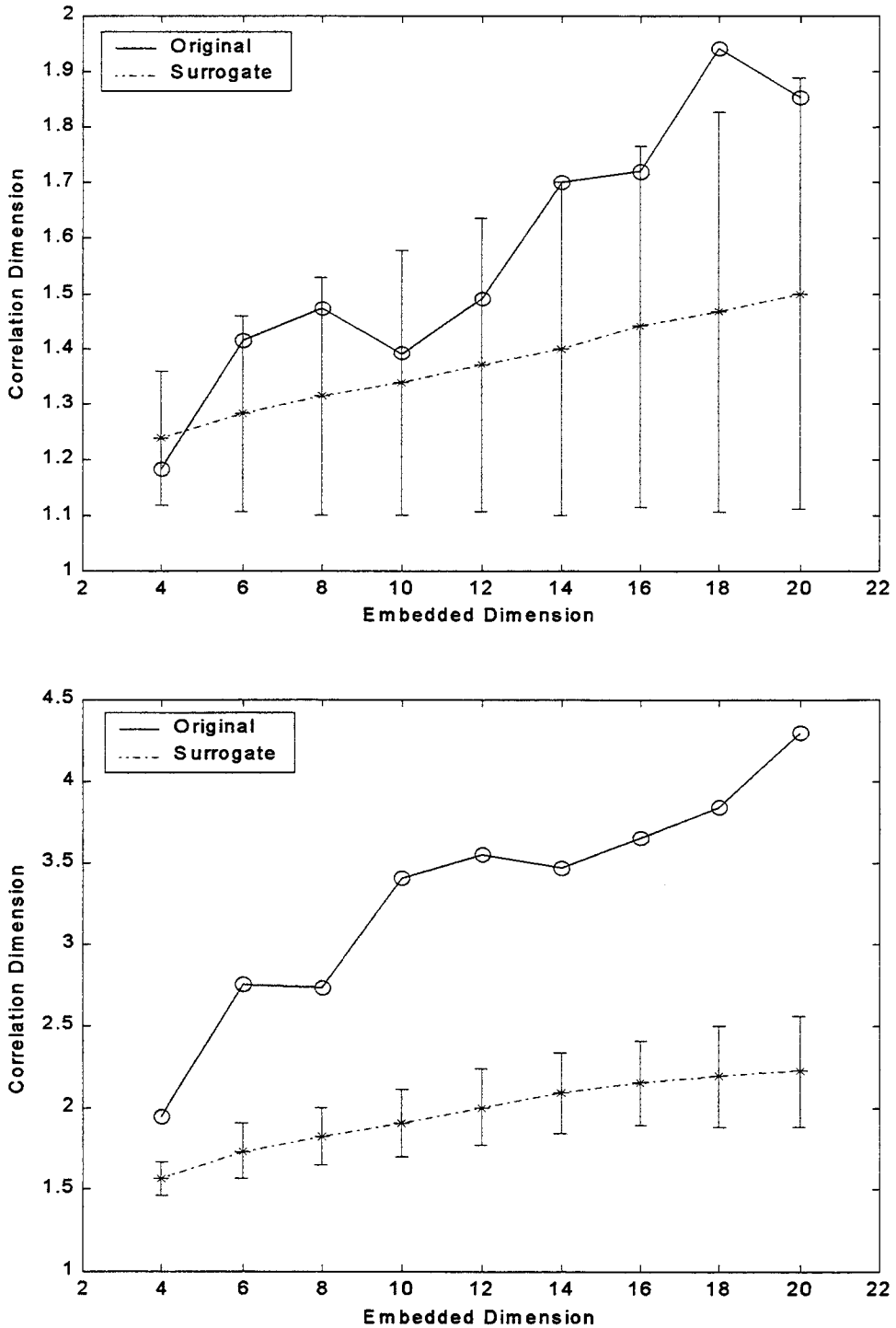

Figure 7.9: Correlation dimension of two subjects from the elderly group. The correlation dimension of the original data and for its corresponding surrogates (and their standard deviation) is plotted vs. the embedded dimension.

Chapter 8

Discussion

8.1 Introduction

In this chapter we examine our results in light of literature available in the field. We will also suggest improvements to our techniques and indicate limitations we have encountered during this study.

8.2 Effect of Age on Physiological Signals Implication: Nonlinear Techniques

We have used power-law scaling (β), approximate entropy (ApEn), and short-term and long term detrended fluctuation analysis (DFA) – for both short-range (α_1) and long-range (α_2) scaling exponents – as indices to characterize the nonlinear dynamics of the HRV signal as well as the effect of age on the autonomic nervous system. While the basic hypothesis that age brings about a change in the nonlinear dynamics of the HRV signal is answered, we believe that these are the optimum indices for the task with the current state of knowledge.

In the light of research conducted by our group and by Pikkujamsa et al. [23], Huikiri et al. [4], Iyengar et al. [24], and Lipsitz [3], we can say with a degree of confidence that power-law scaling (β) is the best predictor of aging and its relation to loss

of complexity. Our findings of heart rate power spectra for healthy young and elderly subjects shows a downward shift and more negative slope of the regression line in the elderly. This observation indicates that relative magnitude is reduced and higher-frequency fluctuations are more attenuated with advancing age.

Pincus et al. [34] proposes that greater regularity or decreased complexity of signals from physiologic processes represent the decoupling of physiological components. This loss of complexity results in the isolation of system components and breakdown of long-range correlations. Since the breakdown of networks within the cardiovascular system impairs its ability to rapidly adapt, a loss of complexity in HR signals may be an important marker of susceptibility to disease. Such loss of complexity is characterized by approximate entropy. Results from our study, are consistent with this hypothesis, since approximate entropy has clearly declined with age. Similar results were observed by Lipsitz [3] and Pikkujamsa et al. [23]. These findings suggest that statistical measures such as ApEn that can summarize complex dynamics, may have diagnostic value in distinguishing patients at risk threatening cardiac disease from those with benign conditions [34].

In the detrended fluctuation analysis (DFA) method, the distribution of spectral characteristics at various frequencies and other features in HR behaviour is measured. Peng et al. [26], Huikiri et al. [4], and Iyengar et al. [24] report a difference between the short range scaling exponents and the longer range for elderly healthy subjects. This loss of fractal organization in heartbeat dynamics may reflect the degradation of the integrated physiological regulatory systems with aging. For healthy young subjects, less crossover

was observed, this implies a balance between many different physiological inputs that operate over different time scales to regulate cardiac cycle times. Our findings are consistent with their results. However, for long-term DFA, we find statistical stability in the short-range scaling exponent for both young and elderly subjects. This suggests that the endocrine systems, metabolic processes, volume shifts causing the long-range fluctuation, are more susceptible to the effect of age than other influences.

Surrogate data testing has been used to detect nonlinearity and chaos in EEG and ECG [54]. We have evaluated the surrogate data testing procedure on mixed sine waves, white noise, and HRV from subjects of different age groups. However, we find that the test fails for several subjects, which shows inconsistency in our results. But, our results agree with those of other groups like Pradhan N. et al [54], Govindan R.B. et al. [50] and Kanters J. K. et al. [58]. We found that the hypothesis that the HRV signal is generated by a linear stochastic process is not always rejected. This result may have been due to the choice of ten as the number of surrogates, which reflects a compromise between reducing the statistical variance in the dimension estimate, and the computational and analytical burden. Even when the hypothesis is rejected, the method of surrogate data can be used to exclude certain classes of stochastic dynamics but a definite positive conclusion of chaos in the experimental data cannot be inferred.

8.3 Limitations

While conducting this study, we have encountered various limitations:

- Long-term recordings contain a high number of ectopics. Such large number of ectopics may produce misleading results when applying nonlinear indices to quantify the HRV signal.
- There is a compromise between reducing the length of HRV data sets and the computation time. Generally, for some algorithms, longer data sets (>1024) require several hours of computation time in a 500MHz Pentium computer.
- Applying techniques to real data may result in inconsistencies between different laboratories and between subjects due to the various factors that may contribute to error – e.g. motion of the subject while HRV is being recorded, or a change in recording may also influence the final results -.

8.4 Future Research

Nonlinear parameters can be applied to various diseases, for instance, before and after myocardial infarction (MI), congestive heart failure (CHF), etc. These indices can also be tested with various change in parameters to test the effect of these parameters on the indices – e.g. the length of data -. Further work may also involve a prediction of mortality.

Chapter 9

Conclusions

There is substantial interest in the analysis of HRV signal in a variety of clinical setting. Such analysis provides an understanding of the neurocardiac regulation in healthy subjects and in patients with a variety of clinical disorders. Many investigators have examined the HRV signal for the presence of chaos. However, concrete physiological mechanisms to ascertain the presence of chaos are still elusive. The hypothesis on which this research is based states that the autonomic function as measured by nonlinear indices of the HRV signal decays with age.

We developed several nonlinear indices to characterize and study the HRV signal. These include power-law scaling (β), approximate entropy (ApEn), detrended fluctuation analysis (DFA), surrogate data analysis and correlation dimension. These indices were tested using both the logistic map and simulated signals. The results of our testing suggest that the algorithms are robust and that with increasing randomness, the nonlinear indices degenerate.

The evaluation of these indices on the HRV data recorded from 93 healthy subjects from various age groups yielded a number of contributions to our knowledge in this field. These are listed below:

1. Nonlinear dynamic indices decay with age as examined using power-law scaling (β) and ApEn.

2. The DFA indices become decoupled with age.
3. The surrogate data techniques suggest that chaos is not always present in healthy control subjects. Further work is needed to identify if chaos is unequivocally present in the HRV signal.

Based upon these results and those of others, we believe that nonlinear dynamics can provide an insight into the functioning of the cardiovascular system. Also, aging progressively diminishes the complexity of the neurocardiac control in healthy human subjects.

BIBLIOGRAPHY

[1] Denton T. A., Diamond G. A., Helfant R. H., Khan S., Karagueuzian H., "Fascinating rhythm: A primer on chaos theory and its application," *Am Heart J* **120**: 1419-40 (Dec. 1990).

[2] Griffiths F., Byrne D., "General practice and the new science emerging from the theories of chaos and complexity," *Br J Gen Pract* **48**:1697-1699 (1998).

[3] Lipstiz L. A., "Age-related changes in the complexity of cardiovascular dynamics: A potential marker of vulnerability to disease," *Chaos* **5** (1): 102-9 (1995).

[4] Huikiri H. V., Makikallio T. H., Peng CK., Goldberger A. L., Hintze U., Moller M., "Fractal Correlation Properties of R-R interval Dynamics and Mortality in Patients With Depressed Left Ventricular Function After an Acute Myocardial Infarction," *Circulation* **101**: 47-53 (2000).

[5] Ho K. L., Moody G. B., Peng CK., Mietus J. E., Larson M. G., Levy D., Goldberger A. L., "Predicting Survival in Heart Failure Case and Control Subjects by Use of Fully Automated Methods for Deriving Nonlinear and Conventional Indices of Heart Rate Dynamics," *Circulation* **96**: 842-8 (1997).

[6] Kurths J., Voss A., Saparin P., Witt A., Kleiner H. J., Wessel N., "Quantitative analysis of heart rate variability," *Chaos* **5** (1): 88-94 (1995).

[7] Glass L., Kaplan D., "Understanding Nonlinear Dynamics," New York: Springer-Verlag (1995).

[8] Berne R. M., Levy M. N., "Principles of Physiology," St. Louis: the C.V. Mosby Company (1990).

[9] Harvey A. M., "Effect of Age on Autonomic Neurocardiac Function in Healthy Males and Females," *Ms. Thesis McMaster University, Dept. Kinesiology* (Aug. 1997).

[10] Barold S. S., "Modern Cardiac Pacing," New York: Future Publishing (1995).

[11] Guevara M. R., Glass L., Shrier A., "Phase-Locked rhythms in periodically stimulated heart cell aggregates," *Am J Physiol* **254**: H1-H10 (1988)

[12] Chialvo D. R., Jalife J., "Nonlinear dynamics of cardiac excitation and impulse propagation," *Nature* **330**: 749-52 (1987)

[13] Ritzenberg A. L., Adam D. R. Cohen R. J., "Period multiplying- evidence for nonlinear behaviour of the canine heart," *Nature* **307**: 159-61 (1984)

[14] Chen P. S., Wolf P. D., Dixon E. G., Danieley N. D., Frazier D. W., Smith W. M., Ideker R. E., "Mechanism of ventricular vulnerability to single premature stimuli in open-chest dogs," *Circ Res* **62**: 1191-209 (1988)

[15] Goldberger A. L., Rigney D. R., Mietus J., Antman E. M., Greenwald S., "Nonlinear dynamics in sudden cardiac death syndrome: heart rate oscillations and bifurcations," *Experienta* **44**: 983-7 (1987)

[16] Shrier A., Dubarsky H., Rosengarten M., Guevara M., Nattel S., Glass L., "Prediction of complex atrioventricular conduction rhythms in humans with use of atrioventricular conduction curve," *Circ* **76**: 1196-205 (1987)

[17] Winfree A. T., "Electrical instability in cardiac muscle: phase singularities and rotors," *J Theor Biol* **138**: 353-405 (1989)

[18] Goldberger A. L., "Fractal variability versus pathologic periodicity: complexity loss and stereotypy in disease," *Persp In Biol & Med* **40(4)**: 543-61 (1997)

[19] Goldberger A. L., "Fractal electrodynamics of the heartbeat," *Ann NY Acad Sci* 402-409

[20] Lipsitz L. A, Goldberger A. L., "Loss of complexity and aging," *JAMA* **267(13)**: 1806-09 (1992)

[21] Lipsitz L. A, Goldberger A. L., Moody G. B., Mietus J., "Spectral Characteristics of Heart Rate Variability Before and During Postural Tilt," *Circ* **81(6)**: 1803-10 (1990)

[22] Lombardi F., Sandrone G., Mortara A., Torzillo D., La Rovere M. T., Signorini M. G., Cerutti S., Malliani A., "Linear and Nonlinear Dynamics of Heart Rate Variability After Acute Myocardial Infarction with Normal and Reduced Left Ventricular Ejection Fraction," *Am J Cardiol* **77**: 1283-88 (1996)

[23] Pikkujamsa S. M., Makikallio T. H., Sourander L. B., Raiha I. J., Puukka P., Skytta J., Peng C. K., Goldberger A. L., Huikiri H. V., "Cardiac Interbeat Interval Dynamics from Childhood to Senescence," *Circ* **100**: 393-399 (1999)

[24] Iyengar N., Peng C. K., Morin R., Lipsitz L. A, Goldberger A. L., "Age –Related Alterations in the Fractal Scaling of Cardiac Interbeat Interval Dynamics," *Am J Physiol* **271(40)**: R1078-1084 (1996)

[25] Peng C. K., Mietus J., Hausdorff J. M., Havlin S., Stanley H. E., Goldberger A. L., "Long-Range Autocorrelations and Non-Gaussian Behaviour of the Heartbeat," *Phys Rev Lett* **70(9)**: 1343-1346 (March 1993)

[26] Peng C. K., Havlin S., Stanley H. E., Goldberger A. L., "Quantification of scaling exponents and crossover phenomena in nonstationary heartbeat time series," *Chaos* **5(1)**: 82-87 (1995)

[27] Makikallio T. H., Hoiber S., Kober L., Torp-Pederson C., Peng C. K., Goldberger A. L., Huikiri V. H., "Fractal Analysis of Heart Rate Dynamics as a Predictor of Mortality in Patients with Depressed Left Ventricular Function After Acute Myocardial Infarction," *Am J Cardiol* **83**: 836-839 (1999)

[28] Peng C. K., Havlin S., Stanley H. E., Goldberger A. L., "Fractal Scaling Properties in Nonstationary Heartbeat time series," *AIP Conference Proceedings* **375**: 615-627 (1996)

[29] Goldberger A. L., Mietus J., Rigney D. R., Wood M. L., Fortney S. M., "Effects of head-down bed rest on complex heart rate variability: response to LBNP testing," *Am Phys Soc* **77(6)**: 2863-69 (1994)

[30] Pincus S., "Approximate entropy as a complexity measure," *Chaos* **5(1)**: 110-116 (1995)

[31] Pincus S., Viscarello R., "Approximate entropy: a regularity measure for fetal heart rate analysis," *Obstet Gynecol* **79**: 249-55 (1992)

[32] Pincus S., Cummins T., Haddad G., "Heart rate control in normal and aborted-SIDS infants," *Am J Physiol* **264(33)**: R638-R646 (1993)

[33] Pincus S., Goldberger A. L., "Physiological time-series analysis: what does regularity quantify," *Am J Physiol* **265(35)**: H1643-H1656 (1994)

[34] Pincus S., Cladstone I. M., Ehrenkranz R. A., "A regularity statistic for medical data analysis," *J Clin Monit* **7**: 335-345 (1991)

[35] Pincus S., "Approximate entropy as a measure of system complexity," *Proc Natl Acad Sci* **88**: 2297-2301 (1991)

[36] Kumar V., Cotran R. S., Robins S. L., "Basic Pathology," Toronto: W. B. Saunders pp 459 (1992)

[37] Fallen E. L., Kamath M. V., "Circadian rhythms of HRV," *Malik M & Camm JA Heart Rate Variability. Armonk NY, Futura*: 293-309 (1995)

[38] Brown T. E., Beightol L. A., Eckberg D. L., "Important influence of respiration on human R-R interval power spectra is largely ignored," *J Appl Physiol* **75**: 2310-7 (1993)

[39] Ori Z., Monir G., Weiss J., Sayhouni X., Singer D. H., "Heart rate variability-frequency domain analysis," *Cardiol Clin* **10**: 499-533 (1992)

[40] Kamath M. V., Fallen E., "Power Spectral Analysis of Heart Rate Variability: A noninvasive signature of cardiac autonomic function," *CRC Biomed Eng* **21**: 245-311 (1993)

[41] Mandell A. J., Shlesinger M. F., "Lost choices, parallelism and topological entropy decrements in neurobiological aging," *Krasner S ed. The Ubiquity of Chaos. Washington DC: American Association for the Advancement of Science*: 35-46 (1990)

[42] Frolkis V. V., Bezrukov V. V., "Aging of the central nervous system," *Interdisciplinary Top Gerontol* **16**: 87-89 (1979)

[43] Kaplan D. T., Furman M. I., Pincus S. M., Ryan S. M., Lipsitz L. A, Goldberger A. L., "Aging and the complexity of cardiovascular dynamics," *Biophys J* **59**: 945-949 (1991)

[44] Ryan S. M., Goldberger A. L., Pincus S. M., Mietus J., Lipsitz L. A, "Gender and age related differences in heart rate dynamics: are women more complex than men?," *JACC* **24(7)**:1700-7 (1994)

[45] Yamasaki Y., Kodama M., Matsuhisa M., Kishimoto M., Ozaki H., Tani A., Ueda N., Ishida Y., Kamada T., "Diurnal heart rate variability in healthy subjects: effects of aging and sex difference," *Am J Physiol* **271(40)**: H303-H310 (1996)

[46] Sakata S., Hayano J., Mukai S., Okada A., Fujinama T., "Aging and spectral characteristics of the nonharmonic component of 24-h heart rate variability," *Am J Physiol* **276(45)**: R1724-R1731 (1999)

[47] Urban R. J., Velduis J. D., Blizzard R. M., Dufau M. L., "Attenuated release of biologically active luteinizing hormone in healthy aging men," *J Clin Invest* **81**: 1020-9 (1988)

[48] Flukiger L., Boivin J. M., Quilliot D., Jeandel C., Zannad F., "Differential effects of aging on heart rate variability and blood pressure variability," *J Gerontol* **54A(5)**: B219-B224 (1999)

[49] Greenspan S. L., Klibanski A., Rowe J. W., Elahi D., "Age-related alterations in pulsatile secretion of TSH: role of dopaminergic regulation," *Am J Physiol* **260**: E486-E491 (1991)

[50] Govindan R. B., Narayanan K., Gopinathan M. S., "On the evidence of deterministic chaos in ECG: surrogate and predictability analysis," *Chaos* **8(2)**: 495-501 (June 1998)

[51] Theiler J., Longlin A., Galdrikian B., Farmer D., "Testing for nonlinearity in time series: the method of surrogate data," *Physica D* **58**: 77-94 (1992)

[52] Theiler J., "On the evidence for low-dimensional chaos in an epileptic electroencephalogram," *Phys Lett A* **196**: 335-341 (1995)

[53] Rapp P. E., Albano A. M., Zimmerman D., Jimenez-Monntano M. A., "Phase-randomized surrogate can produce spurious identification of non-random structure." *Phys Lett A* **192**: 27-33 (1994)

[54] Pradhan N., Sadasivan P. K., "Relevance of surrogate data testing in electroencephalogram analysis," *Phys Rev* **E53**: 2684- 2692 (1996)

[55] Lai Y. C., Lerner D., "Effective scaling regime for computing the correlation dimension from chaotic time series," *Physica D* **115**: 1-18 (1998)

[56] Rombouts S. A. R., Keunen R. W. M., Stam C. J., "Investigation of nonlinear structure in multichannel EEG," *Phys Lett A* **202**: 352-8 (1995)

[57] Grassberger P., Procaccia I., "Measuring the strangeness of strange attractors," *Physica D* **9**:189-208 (1983)

[58] Kanters J. K., Holstein-Rathlou N., Agner E., "Lack of evidence for low-dimensional chaos in heart rate variability," *J Cardiovasc Electrophysiol* **5**: 591-601 (1994

APPENDICES

APPENDIX A:

Forms

Aging & Gender Standards for Heart Rate Variability
Subject Consent Form

- Adrian Harvey, B.Kin, Graduate Student, Dept. Human Biodynamics
- Dr. Mark Kamath, Ph.D, Assistant Professor, Dept. Medicine
- Dr. Neil McCartney, Ph.D, Professor, Dept. Kinesiology

Purpose

To establish heart rate variability standards for normal healthy subjects with respect to age & gender for future use in research & clinical practice.

Outline

Procedure will involve both short term, (approx. 45 minutes), and 24 hour ECG recordings. Prior to the recording subjects will be asked to complete a short subject information sheet & a medical questionnaire, (including a standard noninvasive blood pressure measurement). The purpose of these measures is to ensure that the subject population consists of normal, healthy individuals. The short term procedure will involve a single lead setup, (requiring 3 chest electrodes), capable of recording both ECG, (electrical activity of the heart) & respiration. Recording will involve 20 minutes in the supine position & 10 minutes in the standing position, to assess the acute autonomic cardiovascular response to orthostatic stress, (drop in blood pressure on standing), in healthy subjects. The 24 hour recording will be performed with an Oxford Medilog 4500 holter monitor which can be worn with relative comfort on a belt or a shoulder strap. The monitor utilizes a 2 lead setup, (requiring 5 chest electrodes), and records only ECG. Subjects will also be required to fill out an activity diary listing start and finish times for significant activities, (e.g. meals, sleep, work…), during the recording period. The purpose of this long term recording is to identify any age or gender related differences in the normal circadian rhythm known to exist in heart rate variability. The procedure is noninvasive and has no associated risks, (unless the subject has allergies to adhesives used to hold the electrodes and wires to the skin). Subjects that have difficulty tolerating adhesive bandages or any form of athletic or medical tape should not take part in this study.

All collected data will be stored in the Heart Rate Variability Lab, (3E25), at the McMaster University Medical Center under the supervision of Dr. Mark Kamath, (Assistant Professor, Medicine). Data will be published or submitted for thesis credit in such a manner as to maintain the anonymity of those involved. No names or other information that might be used to identify any subjects will be included in these reports. Research findings will be available to the

subjects upon completion of the project. Subjects who wish to review their data should contact Adrian Harvey at 525-9140 xt27390.
Participation in the study is on a volunteer basis and subjects are free to withdraw themselves as well as any of their previously collected data at any time during the study. Subjects may also choose not to answer any questions, (on the subject information sheet or medical questionnaire), or list any activity, (in the activity diary), if they do not feel comfortable doing so.

I have read & understand the procedures & risks involved in this research & I am aware that I may withdraw myself or any of my data at any time during the study:

Name:_____Signature:_____Date:_____

Witness:_____Signature:_____

Aging & Gender Standards for Heart Rate Variability

Medical Questionnaire

Name:_____ Subject#:_____ Date of Birth:_____ Age:_____

1. Do you smoke, (currently or on a regular basis at any time during the past two years)?

Yes:____ No:____

2. Do you have diabetes?

Yes:____ No:____

3. Is there a history of heart disease in your family?

Yes:____ No:____

If so, Who?, At what age did it start?:

4. Have you ever been diagnosed with, or taken medication for hypertension, (high blood pressure)?

Yes:____ No:____

5. Do you suffer from any form of heart disease, (angina, previous heart attack, valvular disease, congestive heart failure, congenital defects etc.)?

Yes:____ No:____

If so what type?:

6. Have you ever fainted in the last 5 years?

Yes:____ No:____

7. Have you ever had a problem with high blood cholesterol?

Yes:____ No:____

8. Please list all medications currently being taken:

9. Blood Pressure, (SBP/DBP):

Date of recording:_____ Signature:_____

Patient Information Profile
Aging and Gender Standards in Heart Rate Variability

Name: Subject#:
Date of Birth(age): ( )
Date of Recording: Time of Recording:
Gender:M( ) F( ) Height: Weight:

Medications?:

Medical Questionnaire?:Yes( ) No( )

Other Tests:

Acute-supine:Yes( ) No( ) Backup?:Yes( ) No( ) Tape#:
Analyzed?:Yes( ) No( )

Acute-standing:Yes( ) No( ) Backup?:Yes( ) No( ) Tape#:
Analyzed?:Yes( ) No( )

Holter:Yes( ) No( ) Backup?:Yes( ) No( ) Tape#:
Diary?:Yes( ) No( )
Time Domain Analyzed?:Yes( ) No( )
Circadian Analyzed?:Yes( ) No( )

Age And Gender Standards in Heart Rate Variability
Holter Diary

Name: John Doe Subject#: N2696B .

Record start and finish times for the 24 hours during the holter recording, (i.e. Sleep, Meals, Medications, Work, Visits to the bathroom...)

Time (Start-Finish)	Description
10:45-11:00	**Walk to Car**
11:20-11:35	**Coffee**
12:00-12:05	**Bathroom**
1:15-1:55	**Lunch**
3:00-3:45	**Walk to and from store**
4:00-4:05	**Bathroom**
6:10-7:00	**Dinner**
7:15-7:25	**Dishes**
8:25-8:30	**Bathroom**
9:12-9:17	**Bathroom**
10:00-10:15	**Snack**
11:30	**Go to Bed**
3:10-3:15	**Bathroom**
8:25	**Wake up, Get out of bed**
9:30-9:50	**Drive to McMaster, Walk from car to Lab**

APPENDIX B:

Raw Data

Data acquired from pediatric subjects, the results with their corresponding mean and standard deviation.

ID #	Age	β	ApEn	α_1 (1024)	α_2 (1024)	α_1 (8192)	α_2 (8192)
A13061	5	-1.3	1.457	0.68	0.668	0.547	0.984
A10072	6	-0.57	1.534	0.488	0.561		
A12061	6	-0.95	1.455	0.823	0.652	1.239	0.889
A05072	7	-1.31	1.479	0.588	0.766	1.02	0.87
A23082	7	-0.98	1.255	1.059	0.657	1.161	0.806
A19061	8	-1.62	1.346	0.885	0.761	1.263	0.899
A10071	9	-1.59	1.575	0.459	0.535	1.118	0.981
A14081	9		1.482	0.879	0.774	1.137	1.027
D2296A	9	-0.93	1.491	0.755	0.724	0.836	0.886
A16082	10	-1.02	1.544	0.807	0.763	0.89	1.044
A31052	10	-1.01	1.471	0.945	0.54	1.13	1.011
A07062	11	-1.09	1.403	0.619	0.725		
A09081	12	-1.32	1.464	1.146	0.691	1.377	1.01
A27061	12	-0.62	1.573	0.572	0.621	0.89	1.071
A23083	12	-1.98	1.307	0.919	0.728	1.078	1.017

Mean	-1.162	1.455	0.774	0.677	1.052	0.961
S.D.	0.388	0.093	0.204	0.082	0.218	0.081

Data acquired from adolescent subjects, the results with their corresponding mean and standard deviation.

ID #	Age	β	ApEn	α_1 (1024)	α_2 (1024)	α_1 (8192)	α_2 (8192)
D2296B	13	-1.34	1.372	0.587	0.581	0.594	0.915
A05071	13	-1.22	1.4106	0.709	0.585	1.002	1.069
A310595	13	-1.31	1.466	0.713	0.617	1.042	1.058
J1897A	13	-0.98	1.44	1.18	0.611	1.037	0.944
A31071	14	-2.06	1.519	0.768	0.986	1.151	1.113
A51072	14	-1.55	1.352	1.063	0.894	1.197	0.917
A28081	15	-1.02	1.466	0.703	0.704	1.267	1.019
A28061	15		1.397	0.602	0.92	1.291	0.829
A28062	15		1.4707	0.909	0.897	1.265	0.999
J2597B	15	-1.73	1.239	1.04	0.83	1.045	0.926
A02081	16		1.437	1.013	0.778	1.344	1.041
A24072	16	-1.52	1.456	0.702	0.931	1.263	1.007
A24073	16	-0.87	1.552	0.987	0.666	1.438	1.014
A21081	17	-2.03	1.469	0.776	0.959	1.306	0.869
A26071	17	-1.9	1.298	0.908	0.893	1.32	1.148
J2597A	17	-1.78	1.496	0.546	1.092	0.9006	0.9595

Mean	-1.483	1.427	0.825	0.809	1.53	0.989
S.D.	0.399	0.081	0.191	0.162	0.21	0.087

Data acquired from adult subjects, the results with their corresponding mean and standard deviation.

ID #	Age	β	ApEn	α_1 (1024)	α_2 (1024)	α_1 (8192)	α_2 (8192)
F0397A	18	-1.3	1.331	0.836	0.689	1.069	1.046
N0296A	18	-1.65	1.462	0.719	0.859	1.001	0.824
N0596A	18	-1.04	1.427	0.91	0.713	1.15	1.084
N2796A	18		1.414	0.908	0.892	1.3211	1.005
O2896A	18	-1.82	1.424	0.581	0.957	1.05	1.001
O1896A	19	-2.22	1.559	0.532	0.829	0.946	0.919
N2696A	19	-0.45	1.3749	0.909	0.708	1.071	0.94
A17071	20	-0.87	1.538	0.847	0.673		
N0796A	22	-1.69	1.456	0.7	0.784	0.936	0.878
N1896A	22	-1.72	1.459	0.844	0.93	1.116	1.081
N1196A	23	-2.53	1.35	1.073	0.986		
MA1597A	24	-1.25	1.382	1.248	0.799	1.4728	0.968
N1296A	24	-0.78	1.477	0.7123	0.815		
N0696A	24	-0.93	1.343	1.133	0.876	1.334	1.048
N0696A	24	-1.04	1.2141	1.26	0.934	1.334	1.048
MA1297A	24	-2.08	1.092	1.251	0.86	1.1406	0.8962
J1597A	25	-1.42	1.312	0.897	1.058		
MA1697A	25	-2.36	1.4037	0.881	0.862	1.194	0.88
J2897A	26	-1.68	1.473	0.851	0.872	1.0569	1.1267
D0396A	26	-1.63	1.516	0.685	0.633	0.919	0.774
N1496A	27	-1.27	1.3466	1.361	0.757	1.405	0.934
N0996A	27	-1.28	1.349	1.187	0.855	1.233	0.795

Mean	-1.52	1.395	0.923	0.833	1.152	0.958
S.D.	0.58	0.105	0.233	0.107	0.166	0.104

Data acquired from middle age subjects, the results with their corresponding mean and standard deviation.

ID #	Age	β	ApEn	α_1 (1024)	α_2 (1024)	α_1 (8192)	α_2 (8192)
F2597A	31	-2.24	1.309	1.062	1.127	1.326	0.8944
M0697A	33	-1.46	1.287	1.224	0.795	1.275	1.022
O2396A	35	-1.58	1.33	1.11	0.759	1.124	1.047
A0997A	35	-1.77	1.545	0.678	0.904	1.048	1.033
M2597A	37	-2.49	1.182	1.051	1.02	1.221	0.9114
N1996A	37	-1.99	1.46	0.898	0.83	1.379	1.0145
M0397A	37	-2.03	1.422	0.767	0.794		
F1597A	40	-1.61	1.396	0.917	0.824	0.7195	1.0107
MA0997A	42	-1.31	1.517	0.868	0.883	1.455	0.9223
MA1397A	42	-1.83	1.312	1.166	0.948	1.257	1.037
F1597B	44	-1.38	1.255	1.4	0.743	1.234	0.926
A0297A	45	-1.56	1.33	1.309	0.781	1.3029	0.8759
D1996A	45	-2.21	1.285	1.237	0.963	1.238	0.913
A2297A	45	-1.59	1.187	1.442	0.822	1.258	1.2118
A0897A	52	-1.87	1.471	0.534	0.916	1.514	0.921
N2896A	56	-1.82	1.423	1.077	0.929	1.116	1.139
A1597A	56	-1.64	1.472	1.022	0.575	1.211	1.128
A0397B	57	-2.19	1.35	0.856	0.974	0.9868	1.0561
A0397A	58	-1.09	1.327	1.311	0.641	1.425	0.946
A2897A	59	-2.07	1.163	1.36	0.847	1.443	1.0585
A2997A	59	-1.73	1.324	1.372	0.719		

Mean	-1.78	1.349	1.079	0.847	1.238	1.003
S.D.	0.34	0.107	0.252	0.127	0.187	0.092

Data acquired from elderly subjects, the results with their corresponding mean and standard deviation.

ID #	Age	β	ApEn	α_1 (1024)	α_2 (1024)	α_1 (8192)	α_2 (8192)
D1696A	61	-1.3	1.457	0.68	0.668	0.547	0.984
A0297B	62	-0.57	1.534	0.488	0.561		
MA0897A	64	-0.98	1.255	1.059	0.657	1.161	0.806
J3097A	65	-1.62	1.346	0.885	0.761	1.263	0.899
A2197B	65	-1.59	1.575	0.459	0.535	1.118	0.981
J1097A	66		1.482	0.879	0.774	1.137	1.027
MA0697A	66	-0.93	1.491	0.755	0.724	0.836	0.886
F1897A	67	-1.02	1.544	0.807	0.763	0.89	1.044
A1497A	67	-1.01	1.471	0.945	0.54	1.13	1.011
F1397A	68	-1.09	1.403	0.619	0.725		
A2197A	68	-1.32	1.464	1.146	0.691	1.377	1.01
D1096B	68	-0.62	1.573	0.572	0.621	0.89	1.071
D1096A	69	-1.98	1.307	0.919	0.728	1.078	1.017
F1197A	69	-1.24	1.142	1.398	0.674	1.44	1.16
J2297A	69	-2.63	1.255	1.268	0.753	1.314	1.095
D2096A	74	-1.94	1.509	0.848	1.009		
F0797A	74	-2.58	0.973	1.504	0.839	1.186	1.201
J2097A	77	-2.47	1.117	1.229	1.088	1.028	0.979
J3197A	78	-1.91	1.191	0.707	0.901		

Mean	-1.95	1.272	1.138	0.86	1.204	1.076
S.D.	0.6	0.135	0.289	0.172	0.205	0.182